water immersion objective), a Yokogawa CSU-21 confocal scanner unit, either EB-CCD or EM-CCD (C7190 or C9100-12, Hamamatsu Photonics, Hamamatsu, Japan), and a piezo electric driver (P-721.17, Physik Instrumente GmbH & Co. KG, Germany). Using this system, a focal plane image (one optical section) can be taken at 33 ms along the *z*-axis. GFP and Alexa Fluor 568 were simultaneously excited by 488- and 568-nm lasers (Krypton Argon-ion lasers; 643-YB-A01, Melles Griot Laser Group, CA, USA). For the simultaneous monitoring of both fluorescent wavelengths, an emission beam splitter, a W-view Optics (A 4313–11, Hamamatsu Photonics), was installed between the scanner unit and the CCD. The W-view consists of a dichroic mirror of 550 nm, two emission filters, a 510/23-nm band pass filter for GFP and a 590 nm long pass filter for Alexa Fluor 568 excited by light at 568 nm, so that two separate images of GFP and Alexa Fluor 568 fluorescence can be produced at the same time.

Mouse preparation for in vivo imaging

Mice were anaesthetized at least 20 min before the surgical procedure with an intraperitoneal injection of Nembutal (Dainippon Sumitomo Pharma, Osaka, Japan) at a dose of 0.06 mg/g of body weight in an atmosphere of diethyl ether. The mesenteric vascular bed was exposed after making a midline incision in the ventral abdominal wall followed by careful exteriorization. Special precautions were taken not to stretch the mesentery or touch it with metallic instruments. Only one to three different vessels per mouse, 200 to 250 μm in diameter with a shear rate ~100 s^{-1} (2.5 dyn/cm^2) were studied [10]. Segments of exteriorized mesenteric veins 142×107 μm in size were evaluated. During the procedure, the mesentery and viscera were moistened by dropwise addition of preheated saline at 37°C to prevent them from drying. Mice were placed in a supine position on the stage of the intravital fluorescence microscope. Digital video recordings were coded for subsequent blinded analysis. Upon completion of the invasive study on the mesentery vessels, mice were euthanized by anaesthetic overdose.

Intravenous DDAVP administration and VWF secretion

DDAVP, a known stimulant of VWF exocytosis, was administered, although its effect on mice is limited [7]. A dose of 0.3 μg/kg body weight [25] was administered intravenously to GFP-ADAMTS13−/− mice (n=6) and GFP mice (n=4). Using an intravital fluorescence confocal microscopy system, and IPLab software (BD Biosciences Bioimaging, MD, USA), the in vivo kinetics of GFP-expressing platelet adhesion on VECs was evaluated. When more than two platelets were connected to each other and adhered on VECs, these connected platelets were considered as one "platelet string". The numbers of adhered single platelets and of "platelet strings" were counted for each venular segment, and the sum of them was indicated as the "total number". The diameter of each single platelet as well as the length of each "platelet string" were also measured for each venular segment, and their sum was indicated as the "total length". The average lengths were also calculated by dividing "total length" by the "total number". During this experiment, only one vein per mouse was evaluated. The results represent data for an average venular segment, with five segments counted and recorded over the same period of time (100 frames, 30 frames per sec). Recordings were made just before and just after DDAVP administration, in 5-min intervals for up to 1 h. For visualizing VWF multimer strings, Alexa Fluor 568-labeled anti-VWF antibody (0.1 ml of approximately 1 mg/ml solution) was administered intravenously together with DDAVP through the tail vein into GFP-ADAMTS13−/− mice, and the adhesion of GFP-expressing platelets on the strings was confirmed by another set of experiments.

VECs injury by 2.5% ferric chloride ($FeCl_3$)

Mesenteric venules were exteriorized and injured by topical use of $FeCl_3$ solution. Lavage of mesentery by dropwise addition of saline, which was continued after its exteriorization, was stopped for 1 min and then 30 μl of 2.5% $FeCl_3$ was topically applied to the surface of the targeted vessel. After 15 s of exposure of the vein to $FeCl_3$, the mesentery was exposed to saline again and the applied $FeCl_3$ was washed out. Precisely 1 min after application of $FeCl_3$, changes in fluorescent intensity in a standard venular segment were recorded for about 23 s (700 frames taken with a video rate of 30 frames per second). Recorded sequences were evaluated at each frame using IPLab software, and the length of connected platelets aligned as beads on a string ("platelet string") was measured. The duration of each string's binding to a vascular surface was also calculated by multiplying the numbers of sequential frames in which the strings were observed by the frame interval of 0.033 s. One segment per vein, and one to three veins per mouse were assessed in GFP-ADAMTS13−/− mice (n=9) and in GFP mice (n=8).

Laser-induced vessel wall injury and image analysis of microthrombi

The mesenteric venule was exteriorized and the endothelium was focally injured by a 514-nm argon ion laser (543-GS-A03; Melles Griot Laser Group, CA). The laser beam was aimed at the endothelium through the microscope objective lens. The injured area of endothelium, the

diameter of which was approximately 10 μm [20], was kept constant by changing the intensity and duration of laser illumination (typically 140 mW, 5 s). Changes in the fluorescence intensity of GFP-expressing platelets were measured with an EB-CCD camera to monitor thrombus formation.

A z-stack of 25 optical sections (2 μm optical slice thickness), at up to 30 frames per second from the vessel wall to the luminal surface of a thrombus, was captured exactly 15, 30, 45, 120, and 300 s after injury and analyzed using a Yokogawa Real Time 3D Workstation and IPLab software in both GFP-ADAMTS13−/− mice (n=6) and GFP mice (n=6). A freehand-defined region of interest was traced along the outline of GFP–platelet thrombus areas. After blinding, scans were analyzed for fluorescence intensity of GFP using Adobe Photoshop CS2 and Scion Image to measure the area of the thrombus. The size of the thrombus was then calculated based on the fact that the thickness of each plane is 2 μm, and its volume was expressed in μm^3. In another set of experiments, Alexa Fluor 568-labeled anti-VWF antibody was injected intravenously through the tail vein into GFP-ADAMTS13−/− mice (n=4) and GFP mice (n=4) before laser irradiation. The scans were taken at exactly 15, 30, 45, 60, 120, and 300 s after laser injury, and the fluorescent intensity of Alexa Fluor 568 was measured to analyze the localization of VWF in the thrombus.

Statistical analysis

To evaluate the significance of differences between two groups, the parametric Student's T test was used unless otherwise indicated. The non-parametric Mann–Whitney U test was also used when the population was not normally distributed. Differences were considered significant at $P<0.05$.

Results

Characteristics of GFP-ADAMTS13−/− mice

GFP-ADAMTS13−/− mice were viable and fertile, and their blood cell counts were normal (Table 1). Plasma VWF levels in GFP-ADAMTS13−/− mice (0.372±0.069 U/ml, mean±SD, n=12) were approximately 1.4 times higher than those in GFP mice (0.259±0.004 U/ml, mean value±SD, n=10). As noted previously for ADAMTS13−/− mice [5, 6, 31], they did not show any sign of developing spontaneous TTP.

In vivo analyses of platelet adhesion to VECs after DDAVP administration: role of ADAMTS13 in proteolysis of secreted UL-VWF multimers

In both GFP-ADAMTS13−/− mice and GFP mice, some platelets adhered to normal VECs even before DDAVP stimuli. Most of these events were observed as a single platelet adhesion but doublet or triplet platelets, which were connected like beads on strings, were also observed. There was no difference in the number of platelets adhered to VECs between the two animal groups before DDAVP stimuli.

Although the ability of DDAVP to stimulate VWF secretion in mice is controversial, we observed enhanced VWF secretion from VECs in the present study, as was reported before [7]. After DDAVP administration, the number of platelets adhered to VECs increased in both GFP-ADAMTS13−/− mice and in GFP mice, and some of them were attached to each other. A simultaneous injection of Alexa568-labeled anti-VWF antibody revealed that these platelets appeared to attach close to the spots labeled by the anti-VWF antibody (Fig. 1). Several platelets connected and aligned on VWF strings were also observed (Supplement Fig. 1). The numbers of both single platelets and "platelet strings" attached to VECs (total number) in a vascular segment were counted. There was no significant difference in these numbers for the first 20 min, whereas a significant difference was observed thereafter between GFP-ADAMTS13−/− mice and GFP mice, which continued until the end of the observation, i.e., for up to 60 min (Fig. 2a). Administration of DDAVP also significantly increased the "total length" of the attached platelets to VECs, which was obtained as a sum of the diameters of attached single platelets, as well as of the length of each "platelet string" per venular segment in GFP-ADAMTS13−/− mice, while in GFP mice, we did not see a similar response (Fig. 2b). The average length of those in GFP-ADAMTS13−/− mice reached a maximum at 5 min, and these strings were significantly longer than those in the GFP mice (Fig. 2c). Plasma levels of VWF, however, did not significantly increase at 5, 15, 30, 60, or

Table 1 Blood cell counts

	WBC	RBC	Hb	Hct	Plt
GFP-ADAMTS13−/− mice	3650±940	796±23	10.5±0.2	37.1±1.2	46.8±13.0
GFP mice	4950±840	820±44	10.7±0.5	37.4±1.7	42.0±8.9

Mean±SD N=6, *WBC* white blood cells, *RBC* red blood cells, *Hb* hemoglobin, *Hct* hematocrit, *Plt* platelet

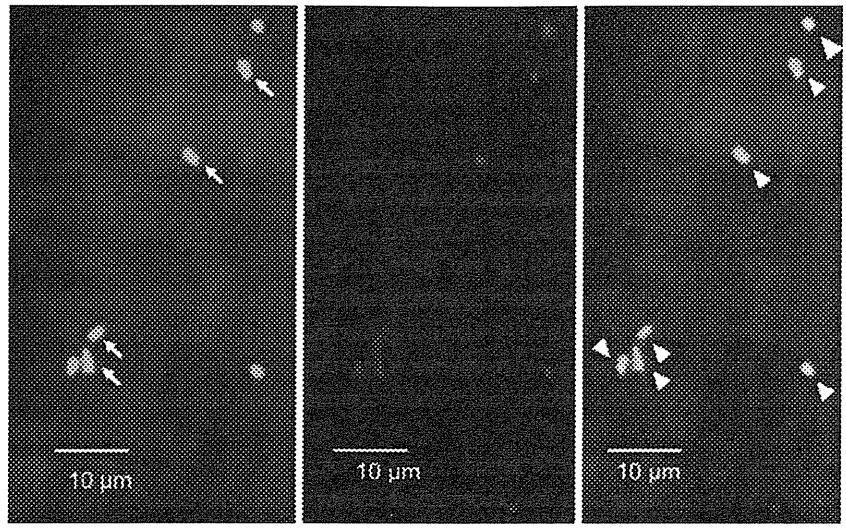

Fig. 1 VWF-dependent platelet adhesion to VECs. A representative figure showing platelets adhered to VECs 25 min after DDAVP administration in GFP-ADAMTS13−/− mice. After intravenous administration of Alexa568-labeled anti-VWF antibody (0.1 ml of 1.0 mg/ml solution) together with DDAVP (0.3 μg/kg body weight), fluorescence of GFP (*green, left*) and Alexa Fluor 568 (*red, middle*) was monitored simultaneously using a W-view system; the right panel is a merged image. Each platelet (*small green dot*) was recognized separately, and some of them were attached (*white arrows*). Most of the spots to which platelets adhered were recognized by Alexa-568-labeled anti-VWF antibody (*white arrow head*). Scale bar shows 10 μm

120 min after DDAVP administration in GFP-ADAMTS13−/− mice or GFP mice (Table 2). The lower dosage of DDAVP employed in the present study, though administered by bolus injection instead of intraperitoneal injection, than previously reported [7] might be a reason for this limited effect.

In vivo analysis of platelets adhesion to $FeCl_3$-injured vascular beds through VWF: role of ADAMTS13 in proteolysis of UL-VWF multimers adhered to an injured vascular wall

$FeCl_3$, at a concentration of 2.5%, induced formation of separated, rather than coalescent, connected platelets aligned on VWF multimer strings, which could be easily evaluated (Fig. 3). The numbers of loci on vascular surfaces injured by $FeCl_3$ to which platelets adhered were similar in GFP-ADAMTS13−/− and GFP mice (46.3±10.2 vs 49.8± 12.3 loci per vascular segment, respectively, mean±SD). The lengths of the adhered strings differed significantly, however, and those in GFP-ADAMTS13−/− mice (mean 25 μm, the 10th–90th percentile 3–50 μm) were approximately 2.5 times longer than those in GFP mice (mean 10 μm, the 10th–90th percentile 2–25 μm, $P<0.01$) (Fig. 4a). The longest string was 105 μm long in GFP-ADAMTS13−/− mice and 50 μm long in GFP mice, respectively. These results reflect the fact that highly active, longer UL-VWF multimers, either circulating in plasma or being secreted from VECs of GFP-ADAMTS13−/− mice, adhered efficiently to the vascular lesion, together with a larger numbers of platelets. Injection of Alexa568-labeled anti-VWF antibody prior to topical use of $FeCl_3$ revealed that multiple strings were bridged by platelets to form longer "platelet strings" (Fig. 5).

The duration time that strings remained attached to the $FeCl_3$-injured vascular surface was measured. The average duration time for VWF strings attached to the vascular surface in the GFP-ADAMTS13−/− mice (mean 1.3 s, the 10th–90th percentile 0.3–6.3 s) was more than four times longer than that for the GFP mice (mean 0.3 s, the 10th–90th percentile 0.2–1.3 s, $P<0.01$) (Fig. 4b). The most stable strings in GFP-ADAMTS13−/− mice survived at least 23.3 s, which was the limit of our observation time in this set of experiments. In GFP mice, the longest string survival time was 6.5 s. These results suggest that the UL-VWF multimers adhered to the vascular lesion were targets for ADAMTS13, and that the lack of this enzyme resulted in sustained adhesion of UL-VWF multimers to the injured vascular wall for longer time periods, together with larger numbers of platelets.

In vivo analysis of microthrombus formation at the laser-induced endothelial injury spot

The process of microthrombus formation at the laser-induced endothelial injury spot was monitored by measuring both the fluorescent intensity of GFP platelets and the size of the thrombi. At each time point, volumes of the thrombi in the group of GFP-ADAMTS13−/− mice tended to be larger than those in the GFP mice, although a significant difference was seen only at 300 s (Fig. 6). The largest thrombi were seen in both groups at 30 s after

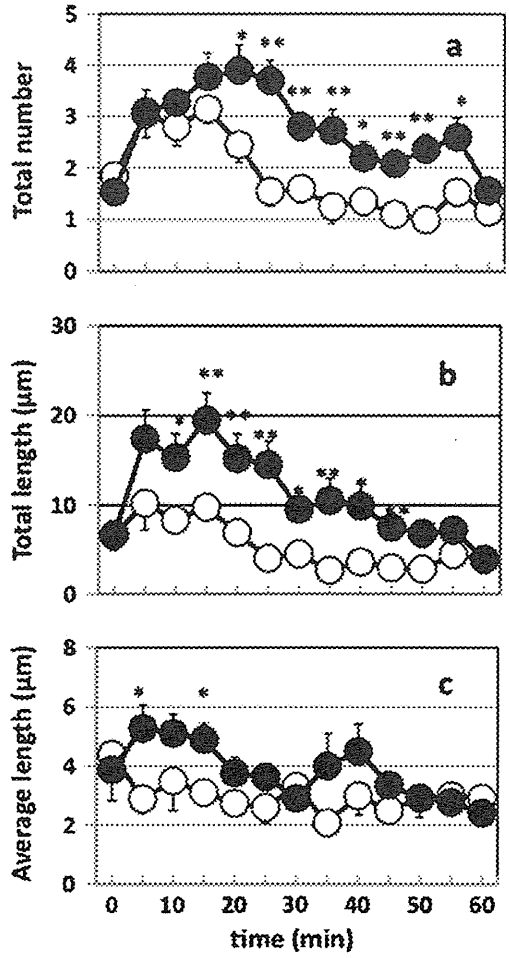

Fig. 2 Platelet adhesion on VECs after DDAVP administration. Numbers of both single platelets and "platelet strings" attached to VECs were counted on each of five venular segments (142×107 μm) of exteriorized mesenteric veins in both GFP-ADAMTS13−/− mice (closed circle, N=6) and GFP mice (open circle, N=4), and results are reported as "total number" (Y-axis, **a**). The diameter of each single platelet as well as the length of each "platelet string" were also measured per venular segment, and results are reported as "total length" (Y-axis, **b**). Their average lengths were calculated in five venular segments (Y-axis, **c**). DDAVP at a dose of 0.3 μg/kg body weight was administered intravenously at point 0. Data are shown as mean±SEM. *P<0.05, **P<0.01

irradiation, and these were 18.8±2.6×10^3 μm^3 in GFP-ADAMTS13−/− mice and 13.1±2.1×10^3 μm^3 in GFP mice, respectively (mean±SEM, n=6) (Fig. 6). The formation of larger thrombi was also shown in an in vitro model

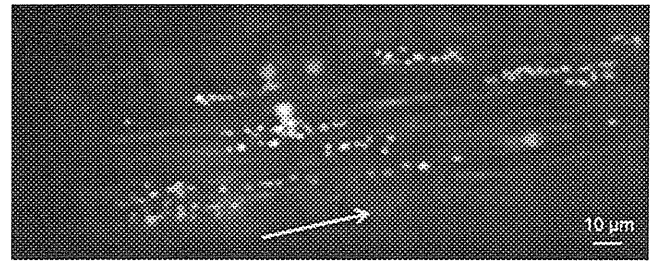

Fig. 3 "Platelet strings" attached to a vascular wall injured by $FeCl_3$. GFP-platelets connected and aligned on a string, i.e., a "platelet string", were observed approximately 1 min after topical application of $FeCl_3$ in GFP-ADAMTS13−/− mice. Application of 2.5% $FeCl_3$ induced separated but not coalescent "platelet string" formation. The continuity of each string was confirmed by evaluating the harmonized motion of connected platelets using digital video images. Scale bar shows 10 μm

after ADAMTS13 depletion using a neutralizing antibody [14]. Differences between the two groups at the laser-induced endothelial injury site, however, appeared smaller when compared with the lengths of "platelet strings" formed on the $FeCl_3$-injured vascular wall. Alexa Fluor 568-labeled anti-VWF antibody was injected to analyze the distribution of VWF in the thrombus in GFP-ADAMTS13−/− mice and in GFP mice. The labeled antibody initially appeared to distribute both in the center and at the periphery of the thrombus, but later it accumulated mainly in the center of the mural-forming thrombus (Fig. 7). A similar distribution was also observed in GFP mice (not shown). The specific binding of this anti-VWF antibody was confirmed by the lack of accumulation of control IgG obtained from non-immunized mice [20]. Bovine serum albumin labeled with Alexa Fluor 568 also did not accumulate in the thrombi (data not shown).

Discussion

Employing ADAMTS13 gene knockout mice expressing GFP, we analyzed the behavior of intact platelets that were not externally manipulated, e.g., by a fluorescent labeling process, on either normal or injured vascular beds in living animals. We found that VWF multimers attached to VECs after stimulation by DDAVP, a secretagogue of VWF

Table 2 Plasma levels of VWF after DDAVP administration

	Sampling time (minutes)				
	0	5	30	60	120
GFP-ADAMTS13−/− mice	0.372±0.069	0.329±0.025	0.340±0.030	0.377±0.011	0.362±0.010
GFP mice	0.259±0.004	0.219±0.066	0.376±0.003	0.326±0.072	0.368±0.029

Mean±SD, N=12 for GFP-ADAMTS13−/− mice and 10 for GFP mice at time 0, N=3–4 for other time points

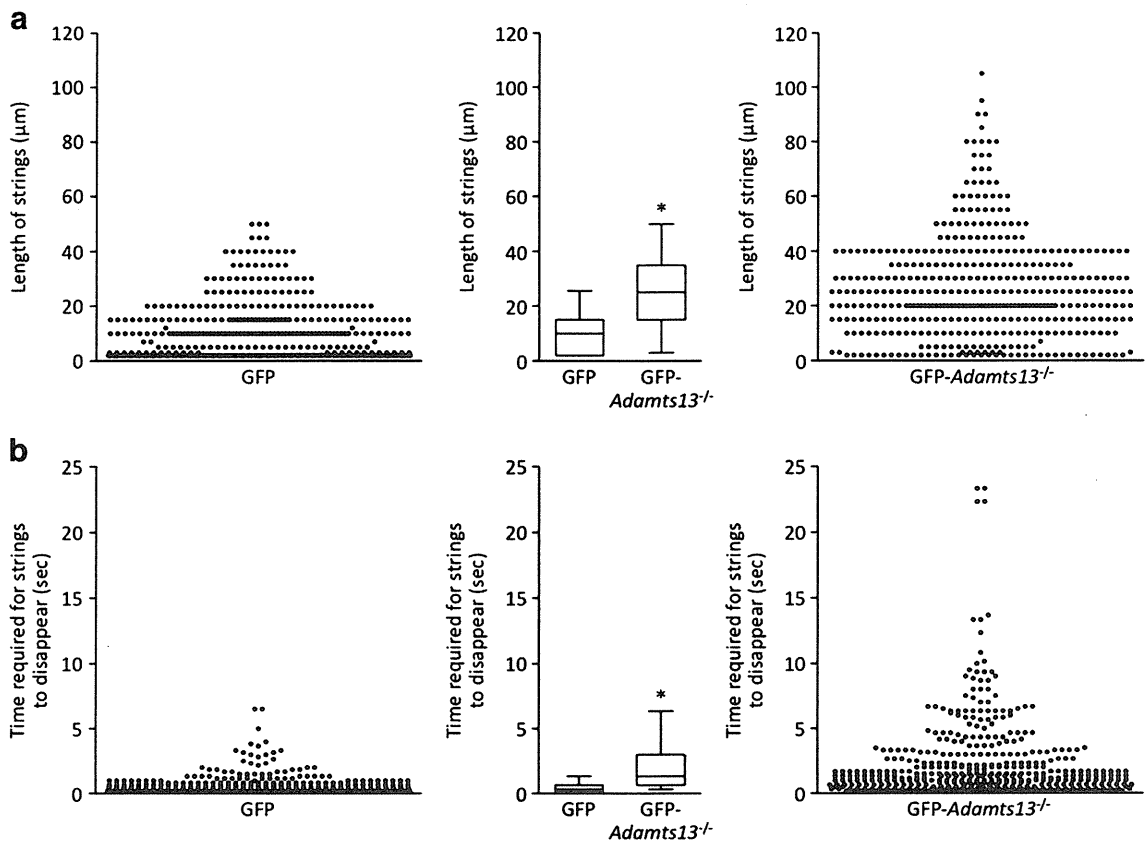

Fig. 4 Quantitative analysis of strings attached to a vascular wall injured by $FeCl_3$. For quantification, 416 strings and 397 strings were observed in GFP-ADAMTS13−/− mice and GFP mice, respectively. The numbers of the strings (*X*-axis) are shown for each length of the strings (*Y*-axis) (**a**). The numbers of strings that disappeared after their initial appearance (*X*-axis) are also shown together with the duration time for VWF strings attached to the vascular surface from their initial appearance (*Y*-axis) (**b**). The length of strings was evaluated when the strings reached their maximum length. The longest persistence times noted were 23.3 s in GFP-ADAMTS13−/− mice and 6.5 s in GFP mice, respectively. Data are also shown as median values together with the values of the 10th and 90th percentiles (*bars*) and of the 25th and 75th percentiles (*boxes*) (**a** and **b**). Statistical significance of differences between the two groups was evaluated by the Mann–Whitney *U* test. **P*<0.01

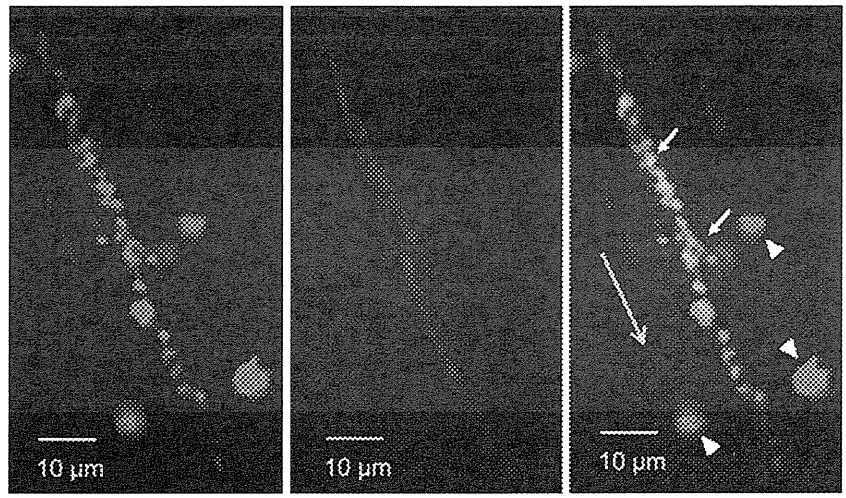

Fig. 5 Elongated UL-VWF multiple strings bridged by platelets. Intravenous administration of Alexa568-labeled anti-VWF antibody followed by topical use of $FeCl_3$ revealed that multiple strings attached to a vascular wall were bridged by platelets to form longer strings in GFP-ADAMTS13−/− mice. Fluorescence of GFP (*green, left*) and Alexa Fluor 568 (*red, middle*) was monitored simultaneously using a W-view system; the right panel is a merged image. Platelets bridging multiple strings are indicated by *white arrows*. White blood cells attached to a vascular wall were also observed (*arrowhead*). The *yellow arrow* shows the direction of blood flow. Scale bar shows 10 μm

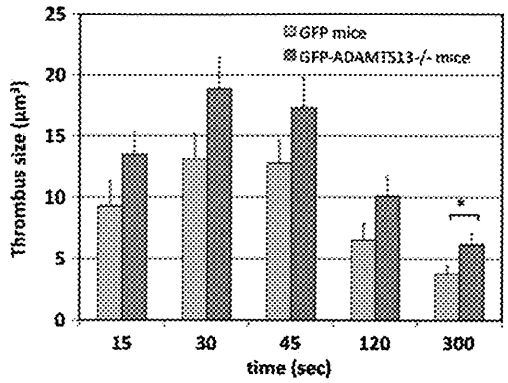

Fig. 6 Size of thrombus formed after laser irradiation. Thrombus formation was triggered by laser irradiation (140 mW, 5 s). Exactly 15, 30, 45, 120, and 300 s after these stimuli, sequences of focal plane images were taken and the area of the thrombus was evaluated by measuring the fluorescent image of GFP platelets. Data are shown as mean±SEM (n=6). *P<0.05

causing its release from storage sites in Weibel-Palade bodies, were longer in GFP-ADAMTS13−/− than in GFP mice, suggesting that ADAMTS13 cleaves UL-VWF multimers during the secretion process, as was previously shown in ADAMTS13−/− mice by stimuli such as histamine and calcium ionophore [10]. Longer platelet strings were also found on the vascular wall after $FeCl_3$ treatment, which is an established technique to expose collagen fibers on the vascular wall by denuding VECs. This suggests that UL-VWF multimers either circulating in plasma or being secreted from VECs of GFP-ADAMTS13−/− mice [6] effectively adhere to the injured vascular wall, together with larger numbers of platelets, compared to GFP mice. Effective and sustained platelet adhesion of long strings composed of several UL-VWF multimers that were bridged by platelets apparently contributed to the accumulation of larger numbers of platelets at the injured vascular wall in ADAMTS13 deficiency.

Several sequential steps are involved in the activation of platelets to form a mural thrombus. The first step is adhesion of platelets to collagen exposed at the injury site, which occurs when VWF binds to GPIbα on the platelet surface [1]. Platelets also adhere to intact or mildly injured VECs, but they detach from these quickly, and repetition of this process is known as rolling [1]. In the present study, the adhesion of non-activated or only minimally activated platelets to VECs was observed at the spots detected using an anti-VWF antibody, following stimulation with DDAVP, a secretagogue known to act on VWF storage sites via V_2 agonist activity [22]. Adhesion of single platelets, as well as several platelets forming "platelet strings", to the spots detected by anti-VWF antibody was observed, consistent with earlier studies [9, 16]. The de novo binding of platelets was also observed upstream of the elongating "platelet strings" whose luminal side tips were already occupied by other platelets (Supplemental Movie and Supplement Fig. 2). Such binding of non-activated or only minimally activated platelets to VWF has been reported previously only under high shear stress conditions in an in vitro study [38], since shear stress-dependent rearrangement of a cryptic binding site in the VWF A1 domain is required before it can bind GPIb [21]. We observed these phenomena in small veins, suggesting that in the secretion of UL-VWF multimers from Weibel-Palade bodies, venous flow is strong enough to alter the conformation of the binding site in the A1 domain. This possibility was suggested in an earlier study [9].

The average length of a "platelet string" adhered to DDAVP-stimulated VECs was approximately 5.3 μm in GFP-ADAMTS13−/− mice and 2.9 μm in GFP mice; this corresponds to 70mers and 38.5mers of VWF, respectively, if we consider the length of one VWF molecule in a multimer to be 75 nm [39]. These correspond to molecular weights of approximately 19,500 and 10,700 kDa, based on

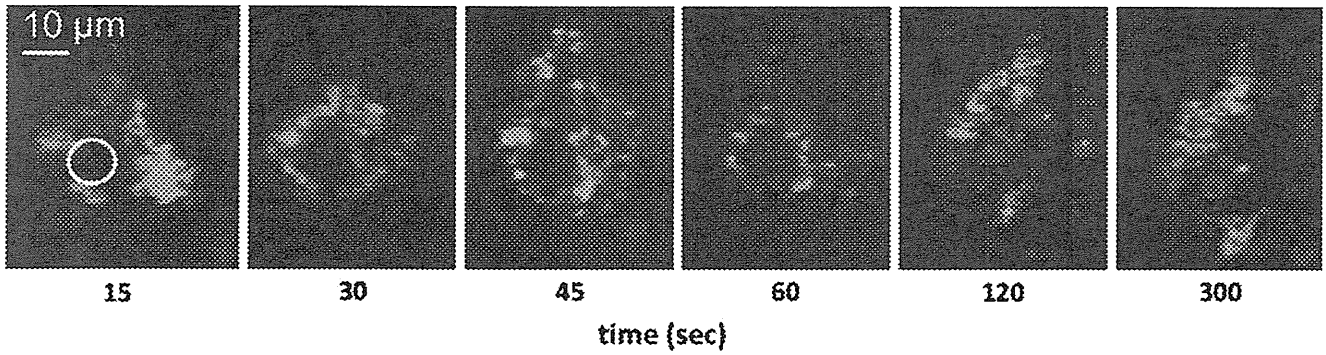

Fig. 7 Localization of VWF in a microthrombus formed by laser irradiation. Accumulation of labeled anti-VWF antibody was evaluated over time as mural thrombi developed in GFP-ADAMTS13−/− mice. The laser-injured area of endothelium is indicated by a *yellow circle* (approximately 10 μm in diameter). Exactly 15, 30, 45, 60, 120, and 300 s after this stimulus, sequences of focal plane images were taken. The focal plane image with the highest intensity of labeled anti-VWF antibody was chosen and evaluated using IPLab software. Scale bar shows 10 μm

the molecular weight of 278 kDa for monomeric VWF [36]. The molecular weight of VWF multimers in normal human subjects ranges from 500 to 20,000 kDa [18]. Thus, the average multimer size in the GFP-ADAMTS13−/− mice was close to the upper limit for UL-VWF in humans, whereas in GFP mice, the average multimer size was within the normal range. The longer length of the platelet strings in GFP-ADAMTS13−/− mice suggests that ADAMTS13 cleaves the UL-VWF multimers even in the vein, which supports a previous in vitro finding that low shear stress is strong enough to cause cleavage of UL-VWF multimers by ADAMTS13 [16]. Thus, lack of ADAMTS13 activity impairs the cleavage of UL-VWF during exocytosis and naturally increases the number of UL-VWF multimers in plasma. The lengths of "platelet strings" adhered to activated VECs by either calcium ionophore or histamine reported previously [10, 31], are similar to those observed after $FeCl_3$ treatment and longer than those observed after DDAVP stimuli in the present study. These results may suggest that DDAVP stimulus is not strong enough to secrete whole VWF strings stored in Weibel-Palade bodies, which can reach 100 μm in length [28]. Another possibility is that the activation of platelet as well as VECs may be required to develop such long strings on VECs in vivo, since both calcium ionophore and histamine are known to enhance platelet aggregation [26].

Next, we examined the behavior of UL-VWF multimers as well as platelets on the injured vascular bed. Exposure of blood vessels to $FeCl_3$, an oxidative chemical agent, is a well-established model of thrombus generation [23]. $FeCl_3$ easily penetrates through the vascular wall and initiates denudation of the endothelium, in which hemolysis and the oxidization of hemoglobin play important roles [45]. The severity of the injury depends on the concentration of $FeCl_3$ as well as the duration of its application to an isolated vein. After trials in which several different concentrations of $FeCl_3$ were applied for different exposure times, $FeCl_3$ application at a concentration of 2.5% for 15 s was chosen, since this procedure produced single and rarely coalescent strings that could be evaluated easily.

After exposure to $FeCl_3$, "platelet strings" were formed on the injured vascular wall, which were longer in GFP-ADAMTS13−/− mice than in GFP mice, although the numbers of the strings were similar. Thus, both UL-VWF multimers circulating in GFP-ADAMTS13−/− mice and VWF multimers having smaller molecular weights in GFP mice adhered to exposed collagen with similar efficacy. Importantly, VWF strings in GFP-ADAMTS13−/− mice remained intact for a longer time than those in the GFP mice. This suggests that UL-VWF multimers bound to the injured vascular wall are cleaved by ADAMTS13 in vivo.

Interestingly, the platelet strings observed following $FeCl_3$ treatment were longer than those observed on VECs after DDAVP stimulation in both groups of animals. The calculated molecular weights of the strings measured following $FeCl_3$ treatment were approximately 96,000 kDa in GFP-ADAMTS13−/− mice and 37,000 kDa in GFP mice, respectively. Thus, they were larger than circulating VWF multimers in plasma, suggesting that multiple strings were bridged by platelets to form longer strings, as shown in Fig. 5. Platelets are highly activated on the injured vascular surface, so it is possible that they bind more tightly to VWF multimers and can form bridges between several VWF strings. In the absence of ADAMTS13 activity, these long strings were hardly cleaved, and therefore the UL-VWF multimers together with large numbers of platelets accumulated at the injured vascular wall. These phenomena were consistent with the pathogenesis of TTP, which is caused by ADAMTS13 deficiency.

Although there were apparent differences between GFP-ADAMTS13−/− mice and GFP mice in the rates at which platelet-bound strings disappeared from the vascular wall, many of the strings in GFP-ADAMTS13−/− mice remained attached temporarily but then disappeared. This raises the question, therefore, of what factors besides ADAMTS13 influence the survival and disappearance of UL-VWF multimer strings adhered to the vascular wall. Dissociation of the multiple UL-VWF strings bridged by platelets through either GPIbα-dependent or GPIIb/IIIa-dependent process is a possible mechanism. Cleavage of UL-VWF multimers by other proteases besides ADAMTS13 might be another mechanism, as suggested previously [8, 33].

To establish the potential role of ADAMTS13 in the ongoing process of mural thrombus generation in vivo, we compared the size of thrombi generated in GFP-ADAMTS13−/− mice and in GFP mice using a laser-induced thrombus model. Thrombi volumes in the GFP-ADAMTS13−/− mice tended to be larger than those in the GFP mice, but these differences were not large. This is in contrast to the striking differences observed between the two groups in the length of "platelet strings" as well as in their adhesion period following $FeCl_3$ treatment. The size of the laser-induced injury on VECs, which is approximately 10 μm, may not be large enough to accurately model the role of UL-VWF multimers at the injured vascular wall in the initiation of a thrombus. We also analyzed the localization of VWF that accumulated in a growing mural thrombus. An Alexa Fluor 568-labeled anti-VWF antibody initially localized to both the center and the periphery of a mural thrombus and then gradually accumulated mainly in its center over time. Recently, we demonstrated that the magnitude of platelet activation varies depending on their location in the thrombus, and that only the platelets in the center of the thrombus are fully activated to express phosphatidylserine on their outer leaflet

[20]. VWF may have accumulated on these activated platelets by binding to GPIIb/IIIa. A similar uneven distribution of VWF was also reported during thrombus formation in an in vitro study [27]. VWF and fibrinogen may play different roles in thrombus formation after binding to GPIIb/IIIa, as was suggested earlier by experiments showing that several GPIIb/IIIa antagonists having distinct abilities to compete for the binding of fibrinogen and VWF to GPIIb/IIIa [2].

In conclusion, in vivo imaging analysis revealed that ADAMTS13 regulates the disappearance of platelet strings on DDAVP-stimulated VECs and on the $FeCl_3$-injured venous vascular wall through the cleavage of UL-VWF. Lack of ADAMTS13 appeared to facilitate the formation of long-lived and elongated platelet strings adhered at the focally injured vascular wall in vivo.

Acknowledgments This work was supported in part by Grants-in-Aid for Scientific Research from the Japan Society for the Promotion of Science (JSPS) (to T.U., Y.S., H.M., F.B., and T.M.), the Ministry of Health, Labor, and Welfare of Japan (to T.M.), the Japan Society for the Promotion of Science (to T.M.), the Program for Promotion of Fundamental Studies in Health Sciences of the National Institute of Biochemical Innovation of Japan (to T.M.), the Smoking Research Foundation (to T.U.), and a scholarship to M.R. from the Ministry of Education, Culture, Sports, Science and Technology of Japan.

Conflicts of interest The authors declare that there are no conflicts of interest associated with study.

References

1. Andrews RK, Berndt MC (2008) Platelet adhesion: a game of catch and release. J Clin Invest 118(9):3009–3011
2. Aoki T, Tomiyama Y, Honda S, Mihara K, Yamanaka T, Okubo M, Moriguchi A, Mutoh S (2005) Association of the antagonism of von Willebrand factor but not fibrinogen by platelet alphaIIb-beta3 antagonists with prolongation of bleeding time. J Thromb Haemost 3(10):2307–2314
3. Asada Y, Sumiyoshi A, Hayashi T, Suzumiya J, Kaketani K (1985) Immunohistochemistry of vascular lesion in thrombotic thrombocytopenic purpura, with special reference to factor VIII related antigen. Thromb Res 38(5):469–479
4. Banno F, Chauhan AK, Kokame K, Yang J, Miyata S, Wagner DD, Miyata T (2009) The distal carboxyl-terminal domains of ADAMTS13 are required for regulation of in vivo thrombus formation. Blood 113(21):5323–5329
5. Banno F, Chauhan AK, Miyata T (2010) The function of ADAMTS13 in thrombogenesis in vivo: insights from mutant mice. Int J Hematol 91(1):30–35
6. Banno F, Kokame K, Okuda T, Honda S, Miyata S, Kato H, Tomiyama Y, Miyata T (2006) Complete deficiency in ADAMTS13 is prothrombotic, but it alone is not sufficient to cause thrombotic thrombocytopenic purpura. Blood 107(8):3161–3166
7. Bovenschen N, Herz J, Grimbergen JM, Lenting PJ, Havekes LM, Mertens K, van Vlijmen BJ (2003) Elevated plasma factor VIII in a mouse model of low-density lipoprotein receptor-related protein deficiency. Blood 101(10):3933–3939
8. Buzza MS, Dyson JM, Choi H, Gardiner EE, Andrews RK, Kaiserman D, Mitchell CA, Berndt MC, Dong JF, Bird PI (2008) Antihemostatic activity of human granzyme B mediated by cleavage of von Willebrand factor. J Biol Chem 283(33):22498–22504
9. Chauhan AK, Goerge T, Schneider SW, Wagner DD (2007) Formation of platelet strings and microthrombi in the presence of ADAMTS-13 inhibitor does not require P-selectin or beta3 integrin. J Thromb Haemost 5(3):583–589
10. Chauhan AK, Motto DG, Lamb CB, Bergmeier W, Dockal M, Plaimauer B, Scheiflinger F, Ginsburg D, Wagner DD (2006) Systemic antithrombotic effects of ADAMTS13. J Exp Med 203 (3):767–776
11. Coller BS, Shattil SJ (2008) The GPIIb/IIIa (integrin alphaIIb-beta3) odyssey: a technology-driven saga of a receptor with twists, turns, and even a bend. Blood 112(8):3011–3025
12. De Marco L, Girolami A, Zimmerman TS, Ruggeri ZM (1986) von Willebrand factor interaction with the glycoprotein IIb/IIa complex. Its role in platelet function as demonstrated in patients with congenital afibrinogenemia. J Clin Invest 77(4):1272–1277
13. Dent JA, Galbusera M, Ruggeri ZM (1991) Heterogeneity of plasma von Willebrand factor multimers resulting from proteolysis of the constituent subunit. J Clin Invest 88(3):774–782
14. Donadelli R, Orje JN, Capoferri C, Remuzzi G, Ruggeri ZM (2006) Size regulation of von Willebrand factor-mediated platelet thrombi by ADAMTS13 in flowing blood. Blood 107(5):1943–1950
15. Dong JF (2005) Cleavage of ultra-large von Willebrand factor by ADAMTS-13 under flow conditions. J Thromb Haemost 3 (8):1710–1716
16. Dong JF, Moake JL, Nolasco L, Bernardo A, Arceneaux W, Shrimpton CN, Schade AJ, McIntire LV, Fujikawa K, Lopez JA (2002) ADAMTS-13 rapidly cleaves newly secreted ultralarge von Willebrand factor multimers on the endothelial surface under flowing conditions. Blood 100(12):4033–4039
17. Falati S, Gross P, Merrill-Skoloff G, Furie BC, Furie B (2002) Real-time in vivo imaging of platelets, tissue factor and fibrin during arterial thrombus formation in the mouse. Nat Med 8 (10):1175–1181
18. Furlan M (1996) Von Willebrand factor: molecular size and functional activity. Ann Hematol 72(6):341–348
19. Furlan M, Robles R, Galbusera M, Remuzzi G, Kyrle PA, Brenner B, Krause M, Scharrer I, Aumann V, Mittler U, Solenthaler M, Lammle B (1998) von Willebrand factor-cleaving protease in thrombotic thrombocytopenic purpura and the hemolytic-uremic syndrome. N Engl J Med 339(22):1578–1584
20. Hayashi T, Mogami H, Murakami Y, Nakamura T, Kanayama N, Konno H, Urano T (2008) Real-time analysis of platelet aggregation and procoagulant activity during thrombus formation in vivo. Pflugers Archiv 456(6):1239–1251
21. Huizinga EG, Tsuji S, Romijn RA, Schiphorst ME, de Groot PG, Sixma JJ, Gros P (2002) Structures of glycoprotein Ibalpha and its complex with von Willebrand factor A1 domain. Science 297 (5584):1176–1179
22. Kaufmann JE, Oksche A, Wollheim CB, Gunther G, Rosenthal W, Vischer UM (2000) Vasopressin-induced von Willebrand factor secretion from endothelial cells involves V2 receptors and cAMP. J Clin Invest 106(1):107–116
23. Kurz KD, Main BW, Sandusky GE (1990) Rat model of arterial thrombosis induced by ferric chloride. Thromb Res 60(4):269–280
24. Levy GG, Nichols WC, Lian EC, Foroud T, McClintick JN, McGee BM, Yang AY, Siemieniak DR, Stark KR, Gruppo R, Sarode R, Shurin SB, Chandrasekaran V, Stabler SP, Sabio H, Bouhassira EE, Upshaw JD Jr, Ginsburg D, Tsai HM (2001) Mutations in a member of the ADAMTS gene family cause

thrombotic thrombocytopenic purpura. Nature 413(6855):488–494
25. Mannucci PM (1997) Desmopressin (DDAVP) in the treatment of bleeding disorders: the first 20 years. Blood 90(7):2515–2521
26. Masini E, Di Bello MG, Raspanti S, Fomusi Ndisang J, Baronti R, Cappugi P, Mannaioni PF (1998) The role of histamine in platelet aggregation by physiological and immunological stimuli. Inflamm Res 47(5):211–220
27. Matsui H, Sugimoto M, Mizuno T, Tsuji S, Miyata S, Matsuda M, Yoshioka A (2002) Distinct and concerted functions of von Willebrand factor and fibrinogen in mural thrombus growth under high shear flow. Blood 100(10):3604–3610
28. Michaux G, Abbitt KB, Collinson LM, Haberichter SL, Norman KE, Cutler DF (2006) The physiological function of von Willebrand's factor depends on its tubular storage in endothelial Weibel-Palade bodies. Dev Cell 10(2):223–232
29. Moake JL, Rudy CK, Troll JH, Weinstein MJ, Colannino NM, Azocar J, Seder RH, Hong SL, Deykin D (1982) Unusually large plasma factor VIII:von Willebrand factor multimers in chronic relapsing thrombotic thrombocytopenic purpura. N Engl J Med 307(23):1432–1435
30. Moake JL, Turner NA, Stathopoulos NA, Nolasco LH, Hellums JD (1986) Involvement of large plasma von Willebrand factor (vWF) multimers and unusually large vWF forms derived from endothelial cells in shear stress-induced platelet aggregation. J Clin Invest 78(6):1456–1461
31. Motto DG, Chauhan AK, Zhu G, Homeister J, Lamb CB, Desch KC, Zhang W, Tsai HM, Wagner DD, Ginsburg D (2005) Shigatoxin triggers thrombotic thrombocytopenic purpura in genetically susceptible ADAMTS13-deficient mice. J Clin Invest 115(10):2752–2761
32. Okabe M, Ikawa M, Kominami K, Nakanishi T, Nishimune Y (1997) 'Green mice' as a source of ubiquitous green cells. FEBS Lett 407(3):313–319
33. Raife TJ, Cao W, Atkinson BS, Bedell B, Montgomery RR, Lentz SR, Johnson GF, Zheng XL (2009) Leukocyte proteases cleave von Willebrand factor at or near the ADAMTS13 cleavage site. Blood 114(8):1666–1674
34. Rieger M, Ferrari S, Kremer Hovinga JA, Konetschny C, Herzog A, Koller L, Weber A, Remuzzi G, Dockal M, Plaimauer B, Scheiflinger F (2006) Relation between ADAMTS13 activity and ADAMTS13 antigen levels in healthy donors and patients with thrombotic microangiopathies (TMA). Thromb Haemost 95 (2):212–220
35. Ruggeri ZM (2002) Platelets in atherothrombosis. Nat Med 8 (11):1227–1234
36. Ruggeri ZM, Ware J (1993) von Willebrand factor. FASEB J 7 (2):308–316
37. Sadler JE (2005) von Willebrand factor: two sides of a coin. J Thromb Haemost 3(8):1702–1709
38. Savage B, Saldivar E, Ruggeri ZM (1996) Initiation of platelet adhesion by arrest onto fibrinogen or translocation on von Willebrand factor. Cell 84(2):289–297
39. Singh I, Shankaran H, Beauharnois ME, Xiao Z, Alexandridis P, Neelamegham S (2006) Solution structure of human von Willebrand factor studied using small angle neutron scattering. J Biol Chem 281(50):38266–38275
40. Soejima K, Mimura N, Hirashima M, Maeda H, Hamamoto T, Nakagaki T, Nozaki C (2001) A novel human metalloprotease synthesized in the liver and secreted into the blood: possibly, the von Willebrand factor-cleaving protease? J Biochem 130(4):475–480
41. Sporn LA, Marder VJ, Wagner DD (1986) Inducible secretion of large, biologically potent von Willebrand factor multimers. Cell 46(2):185–190
42. Tsai HM, Lian EC (1998) Antibodies to von Willebrand factor-cleaving protease in acute thrombotic thrombocytopenic purpura. N Engl J Med 339(22):1585–1594
43. Uemura M, Tatsumi K, Matsumoto M, Fujimoto M, Matsuyama T, Ishikawa M, Iwamoto TA, Mori T, Wanaka A, Fukui H, Fujimura Y (2005) Localization of ADAMTS13 to the stellate cells of human liver. Blood 106(3):922–924
44. Wagner DD, Olmsted JB, Marder VJ (1982) Immunolocalization of von Willebrand protein in Weibel-Palade bodies of human endothelial cells. J Cell Biol 95(1):355–360
45. Woollard KJ, Sturgeon S, Chin-Dusting JP, Salem HH, Jackson SP (2009) Erythrocyte hemolysis and hemoglobin oxidation promote ferric chloride induced vascular injury. J Biol Chem 284(19):13110–13118
46. Zhang X, Halvorsen K, Zhang CZ, Wong WP, Springer TA (2009) Mechanoenzymatic cleavage of the ultralarge vascular protein von Willebrand factor. Science 324(5932):1330–1334
47. Zhang Q, Zhou YF, Zhang CZ, Zhang X, Lu C, Springer TA (2009) Structural specializations of A2, a force-sensing domain in the ultralarge vascular protein von Willebrand factor. Proc Natl Acad Sci USA 106(23):9226–9231
48. Zheng X, Chung D, Takayama TK, Majerus EM, Sadler JE, Fujikawa K (2001) Structure of von Willebrand factor-cleaving protease (ADAMTS13), a metalloprotease involved in thrombotic thrombocytopenic purpura. J Biol Chem 276(44):41059–41063
49. Zhou W, Inada M, Lee TP, Benten D, Lyubsky S, Bouhassira EE, Gupta S, Tsai HM (2005) ADAMTS13 is expressed in hepatic stellate cells. Lab Invest 85(6):780–788

Neurol Sci
DOI 10.1007/s10072-011-0913-9

ORIGINAL ARTICLE

ADAMTS13 gene deletion enhances plasma high-mobility group box1 elevation and neuroinflammation in brain ischemia–reperfusion injury

Masayuki Fujioka · Takafumi Nakano · Kazuhide Hayakawa · Keiichi Irie · Yoshiharu Akitake · Yuya Sakamoto · Kenichi Mishima · Carl Muroi · Yasuhiro Yonekawa · Fumiaki Banno · Koichi Kokame · Toshiyuki Miyata · Kenji Nishio · Kazuo Okuchi · Katsunori Iwasaki · Michihiro Fujiwara · Bo K. Siesjö

Received: 13 August 2011 / Accepted: 20 December 2011

Abstract Highly adhesive glycoprotein von Willebrand factor (VWF) multimer induces platelet aggregation and leukocyte tethering or extravasation on the injured vascular wall, contributing to microvascular plugging and inflammation in brain ischemia–reperfusion. A disintegrin and metalloproteinase with thrombospondin type-1 motifs 13 (ADAMTS13) cleaves the VWF multimer strand and reduces its prothrombotic and proinflammatory functions. Although ADAMTS13 deficiency is known to amplify post-ischemic cerebral hypoperfusion, there is no report available on the effect of ADAMTS13 on inflammation after brain ischemia. We investigated if ADAMTS13 deficiency intensifies the increase of extracellular HMGB1, a hallmark of post-stroke inflammation, and exacerbates brain injury after ischemia–reperfusion. ADAMTS13 gene knockout (KO) and wild-type (WT) mice were subjected to 30-min middle cerebral artery occlusion (MCAO) and 23.5-h reperfusion under continuous monitoring of regional cerebral blood flow (rCBF). The infarct volume, plasma high-mobility group box1 (HMGB1) level, and immunoreactivity of the ischemic cerebral cortical tissue (double immunofluorescent labeling) against HMGB1/NeuN (neuron-specific nuclear protein) or HMGB1/MPO (myeloperoxidase) were estimated 24 h after MCAO. ADAMTS 13KO mice had larger brain infarcts compared with WT 24 h after MCAO ($p < 0.05$). The rCBF during reperfusion decreased more in ADAMTS13KO mice. The plasma HMGB1 increased more in ADAMTS13KO mice than in WT after ischemia–reperfusion ($p < 0.05$). Brain ischemia induced more prominent activation of inflammatory cells co-expressing HMGB1 and MPO and more marked neuronal death in the cortical ischemic penumbra of ADAMTS13KO mice. ADAMTS13 deficiency may enhance systemic and brain inflammation associated with HMGB1 neurotoxicity, and aggravate brain damage in mice after brief focal ischemia. We hypothesize that ADAMTS13 protects brain from ischemia–reperfusion injury by regulating VWF-dependent inflammation as well as microvascular plugging.

Keywords Brain ischemia–reperfusion · High-mobility group box1 · ADAMTS13 · Inflammation · Von Willebrand factor · Thrombotic thrombocytopenic purpura

M. Fujioka (✉) · T. Nakano · K. Hayakawa · K. Irie · Y. Akitake · Y. Sakamoto · K. Mishima · C. Muroi · K. Iwasaki · M. Fujiwara
Department of Neuropharmacology, Faculty of Pharmaceutical Sciences, Fukuoka University, Fukuoka, Japan
e-mail: mfujioka_2000_99@yahoo.co.jp

M. Fujioka
Stroke Center, Helios General Hospital Aue, Dresden University of Technology, Dresden, Saxony, Germany

M. Fujioka · C. Muroi · Y. Yonekawa
Department of Neurosurgery, University of Zurich, Zurich, Switzerland

M. Fujioka · K. Nishio · K. Okuchi
Emergency and Critical Care Medical Center, Nara Medical University, Nara, Japan

K. Irie · Y. Akitake · K. Mishima · C. Muroi · K. Iwasaki
Institute for Aging and Brain Sciences, Fukuoka University, Fukuoka, Japan

F. Banno · K. Kokame · T. Miyata
Research Institute, National Cerebral and Cardiovascular Center, Suita, Japan

B. K. Siesjö
Laboratory for Experimental Brain Research, Lund University, Lund, Sweden

Published online: 03 January 2012

Introduction

The post-ischemic inflammation incites stroke evolution [15, 16, 19–21, 32]. An ischemic insult triggers leukocytes infiltration and astrocyte and microglia activations in the affected brain, leading to the increase of the high-mobility group box1 (HMGB1) in the plasma and brain of the stroke model [19, 21]. The HMGB1 is a potent proinflammatory cytokine secreted by blood-immune [23, 29, 45] and brain-glial cells [35]. This extracellular HMGB1 further activates monocytes/macrophages [3, 34], neutrophils [1, 34], microvascular endothelial cells [12], astrocytes [36] and microglia [24], amplifies the systemic and brain inflammation, and extends the ischemic brain damage into the penumbra [19, 21, 24, 27, 33, 38].

Within the ischemic brain vasculature after middle cerebral artery occlusion (MCAO), circulating platelets [2, 28] and leukocytes [9, 28, 31] are activated, inducing microvascular obstructions and inflammation. In the initial activations of platelet and leukocyte on ischemic endothelium, a large multimeric adhesive glycoprotein von Willebrand factor (VWF) plays a central role. The VWF multimer tethers platelets on the vascular endothelial surface, leading to platelet activation [40]. This platelet-decorated VWF multimer string bound to endothelium supports leukocytes tethering, rolling and transmigration on stimulated vascular endothelial cells, and links thrombosis to inflammation [5, 7, 37]. The platelet binding affinity of VWF increases with increasing length of the VWF multimer strand and with high fluid shear stress [40, 44]. Accordingly, the longest multimer termed ultra-large VWF (ULVWF; secreted by vascular endothelium upon stimulation) exerts its maximum prothrombotic and pro-inflammatory functions in the microvasculture or stenotic vessels under high shear stress condition [30, 40, 41, 43].

A disintegrin and metalloproteinase with thrombospondin type-1 motifs 13 (ADAMTS13) inhibits these VWF functions by cleaving the Tyr1605–Met1606 bond in the A2 domain of the VWF [13, 41]. Physiologically, circulating ADAMTS13 cleaves the ULVWF secreted from endothelial cells, releasing tethered platelets and VWF fragments [11]. In a setting of on-going thrombus formation, the high shear stress induced at the stenotic vasculature stretches plasma-derived VWF multimers (smaller than ULVWF) on the thrombus surface. The extended VWF multimers involved in the platelet thrombosis are consequently cleaved by ADAMTS13 [41]. Notably, by decreasing the interaction between the ULVWF–platelet strands and leukocytes, ADAMTS13 reduces leukocytes adhesion and extravasation on the stimulated vascular wall and down-regulates tissue inflammation [5, 7, 37]. ADAMTS13 deficiency in humans increases the circulating ULVWF resulting in thrombotic thrombocytopenic purpura (TTP) [17, 41]. The TTP manifests fever and neurological deficits associated with VWF–platelet microthrombus formation in the brain. This implies that ADAMTS13 plays a role in inflammation after brain ischemia in TTP patients.

Early studies have shown that ADAMTS13 deficiency aggravates ischemic brain damage in experimental stroke models [14, 48]. We revealed that in the ADAMTS13-deficient mice after a brief focal ischemia the post-ischemic hypoperfusion was significantly amplified partly because of enhanced microvascular plugging by VWF–platelet–leukocyte complex [14]. However, it still remains unclear if an enhanced inflammatory reaction is involved in the deterioration of ischemic brain injury under ADAMTS13 deficiency. Here, we investigated whether ADAMTS13 gene deletion intensifies the increase of extracellular HMGB1, a hallmark of post-stroke inflammation, and exacerbates the brain damage after ischemia–reperfusion.

Materials and methods

Animals

The effect of ADAMTS13 gene deletion on inflammation after brain ischemia was investigated using male ADAMTS13KO and littermate WT mice in an SV129 genetic background, originally generated as a TTP model by our study group [4]. Studies using KO ($n = 31$) and WT ($n = 31$) mice (8–10 weeks of age, 20–23 g of body weight) were approved by the institutional ethics committee. The genotype of each animal was kept unspecified until all experiment's completion.

Middle cerebral artery occlusion

Thirty-minute MCAO by thread insertion from the common carotid artery was induced in KO ($n = 21$) and WT ($n = 21$) mice as previously described [14, 19–21]. Mice were anesthetized with 2% halothane for induction and maintained on 1% halothane in 70% N_2O and 30% O_2 by face mask. Body temperature was maintained at 36.5–37.0°C during surgery. Successful left MCAO was confirmed according to the following criteria: (1) rCBF in the left cerebral cortex at the thread insertion less than 20% of the pre-MCAO rCBF, and (2) consistent presence of significant ischemic neurological symptoms of the left cerebral hemisphere, characterized by right paresis and right circling behavior, during 30-min MCAO. The MCAO surgery was performed within 7 min without bleeding. The anesthesia was discontinued during 30-min MCAO. There were no statistically significant differences in body temperature between the two groups immediately before or after the thread insertion, or 10, 20, and 30 min after

MCAO. The thread was removed under re-anesthesia after 30-min MCAO. Sham surgery in KO ($n = 10$) and WT ($n = 10$) involved temporary insertion (1 s) of the thread into the left common carotid artery without MCAO. There were no statistical differences in prothrombin time or survival rate between KO and WT mice at 24 h after MCAO (Table 1).

Regional cerebral blood flow

The rCBF was measured by laser Doppler flowmetry (LDF) (ALF21, Advance Co., Tokyo, Japan) as previously described [14, 20]. The LDF probe was placed through a guide cannula into the left cerebral cortex stereotaxically (0.22 mm posterior and 2.5 mm lateral from bregma; 1.5 mm depth from the skull surface) on a stereotaxic instrument (Narishige Scientific Instrument Lab: SR-5 M, Tokyo) under anesthesia (pentobarbital 50 mg/kg, i.p.) 24 h before MCAO or sham surgery. The rCBF was monitored in all animals continuously from 30 min before MCAO until immediately after reperfusion. In randomly selected animals, the rCBF was repeatedly recorded over time within 24 h after MCAO. The rCBF during occlusion and reperfusion was expressed as percentages of the preMCAO LDF baseline value.

Infarct volume and neurological deficit

The brains were sectioned coronally (four 2-mm thick slices) according to a mouse brain matrix 24 h after MCAO (KO, $n = 14$ and WT, $n = 15$) or sham operation (KO, $n = 5$ and WT, $n = 5$). The infarct area was measured in each slice stained with 2,3,5 triphenyltetrazolium chloride with an image analysis system (NIH Image, version 1.63), and the infarct volume was calculated [14, 19–21]. Neurological deficit score ranging from 0 (normal motor function) to 5 (no spontaneous motor activity) was measured at 24 h after MCAO [14, 19, 21] (Table 1).

Plasma HMGB1 measurement

The plasma HMGB1 protein was evaluated by western blot 24 h after MCAO. Plasma samples were fractionated by sodium dodecyl sulfate (SDS)-polyacrylamide gel electrophoresis, and HMGB1 levels were determined by immunoblotting with respect to a standard curve, with recombinant HMGB1 as a reference (Sigma-Aldrich, Tokyo) [19, 21]. A blood sample (500 μL) was taken from each experimental animal via inferior vena cava 24 h after MCAO (KO, $n = 11$ and WT, $n = 12$) or sham surgery (KO, $n = 10$ and WT, $n = 10$). The sample was centrifuged (3,000 rpm at 4°C for 10 min), and the supernatant (200 μL) was further centrifuged (15,000 rpm at 4°C for 20 min). SDS sample buffer [125 mmol/L Tris (pH 6.8), 2% SDS, 20% glycerol, 0.0001% bromophenol blue, and 10% β-mercaptoethanol] (100 μL) was added to the plasma extract solution (100 μL), and the resultant sample was heated at 95°C for 5 min. Protein (15 μg) was separated by SDS–polyacrylamide gel electrophoresis (20% gel). Blotting was performed at 2 mA/cm^2 by semi-dry type blotting (Bio-Rad, Tokyo, Japan). The blots were blocked with 5% non-fat dry milk in Tris-buffered saline in 0.1% Tween 20 (TBS-T) at 4°C and incubated with goat polyclonal anti-HMGB1 primary antibody (1:200) (Santa Cruz Biotechnology, Santa Cruz, CA, USA) in TBS-T, followed by bovine anti-goat IgG (heavy chain and light chain [H + L]) alkaline phosphatase conjugate (1:1000) in TBS-T. The blots were visualized with the use of alkaline phosphatase color reagents. The signal intensity of the blots was measured with an image analysis system (NIH Image, version 1.63).

Double immunohistochemical staining for HMGB1/NeuN and HMGB1/MPO

Double immunofluorescent labeling for HMGB1 with NeuN or MPO on paraffin-embedded 5-μm coronal sections

Table 1 Effect of ADAMTS13 gene deletion on brain ischemia in mice after 30-min MCAO and 23.5-h reperfusion

	WT		KO
Brain infarct volume (mm^3)	12.0 ± 2.0 ($n = 15$)	$p < 0.05$[a]	28.5 ± 5.8 ($n = 14$)
Neurological deficit score	1.3 ± 0.2 ($n = 15$)	$p < 0.05$[a]	1.9 ± 0.2 ($n = 14$)
Prothrombin time (s)	12.1 ± 0.8 ($n = 7$)	ns	11.6 ± 0.9 ($n = 6$)
Survival rate (%)	95.2 ($n = 20/21$)	ns	90.4 ($n = 19/21$)

The values are expressed as the mean ± SEM. Neurological deficit score, score 0; normal motor function, 1; flexion of torso and of contralateral forelimb upon lifting of the animal by the tail, 2; circling to the ipsilateral side but normal posture at rest, 3; circling to the ipsilateral side, 4; rolling to the ipsilateral side, 5; leaning to the ipsilateral side at rest (no spontaneous motor activity)

ns Statistically not significant

[a] Student *t* test

of the mouse brain was analyzed by fluorescence microscopy (Nikon, AZ-FL, Tokyo, Japan). At 24 h after MCAO (KO, $n = 5$; WT, $n = 5$) or sham surgery (KO, $n = 5$; WT, $n = 5$), mice were humanely perfused transcardially with saline and 4% paraformaldehyde. The brains were removed of fat and water using an autodegreasing unit (RH-12; Sakura Seiko Co, Tokyo) and embedded in paraffin. Subsequently, 5-μm sections were mounted on slides and dried at 37°C for 1 day. After deparaffinization and rehydration, the sections were incubated with primary antibodies of biotinylated anti-mouse NeuN (1:200; Chemicon International, Temecula, CA, USA) or rabbit polyclonal anti-MPO (1:200; DAKO Inc., Carpinteria, CA, USA) and of goat polyclonal anti-HMGB1 (1:200; Santa Cruz Biotechnology, Santa Cruz, CA, USA) overnight at 4°C. Sections were then incubated with donkey anti-goat IgG-FITC secondary antibody (1:200; Santa Cruz Biotechnology) for 1 h, and thereafter with goat anti-rabbit IgG-Texas red secondary antibody (1:200; Santa Cruz Biotechnology) or Ultra avidine Texas Red (1:200; Leinco Technologies) for 1 h. The sections were imaged and analyzed. The histological findings were evaluated by neuropathologists until a consensus was obtained. The fluorescence intensity (for cells positive to NeuN, MPO, or HMGB1) in five randomly selected areas (150 μm × 200 μm for each) from the region of interest in the ischemic cerebral cortex (as indicated in Figs. 2, 3) was evaluated with an image analysis system (NIH Image, version 1.63) with the corresponding non-ischemic contralateral regions as a control, and the relative fluorescence intensity was calculated. In ischemic stroke, the necrotic core is surrounded by a zone of reactive/inflammatory cytosis which can extend the initial insult into the penumbra with delayed cell death. Based on this concept, the region of interest in the cortical penumbra for the fluorescence evaluation was decided as indicated.

Statistical analysis

Data are presented as mean ± standard error of mean (SEM). For multiple pairwise comparisons in parametric analysis, two-way analysis of variance (ANOVA) followed by Tukey–Kramer's test was performed. When only two groups were compared, Student's *t* test was used. Probability values of <0.05 were considered statistically significant.

Results

Brain infarction

The ADAMTS13 gene knockout (ADAMTS13KO) mice group had a significantly larger volume of brain infarction compared with the wild-type (WT) following 23.5-h reperfusion after 30-min MCAO (Student's *t* test) (Table 1). No ischemic brain damage was observed in either KO or WT mice after sham operation.

Neurological deficits

ADAMTS13KO mice had more severe neurological deficits than the WT (Student's *t* test) 24 h after MCAO (Table 1).

Regional cerebral blood flow

The rCBF showed no statistical differences between the two groups during MCAO or immediately after reperfusion. However, the rCBF in ADAMTS13KO mice progressively decreased significantly more markedly compared to WT during the first 30-min reperfusion (Tukey–Kramer's test). 24 h after MCAO, the rCBF in KO mice remained significantly lower compared to WT (Student's *t* test) (Table 2).

ADAMTS13 gene deletion enhances post-ischemic increase of plasma HMGB1

A 30-min MCAO and 23.5-h reperfusion significantly increased the plasma HMGB1 level both in ADAMTS13KO and WT mice as compared to sham operation (Fig. 1). However, this increase of plasma HMGB1 after MCAO was more markedly enhanced in ADAMTS13KO mice than in WT (Tukey–Kramer's test).

ADAMTS13 gene deletion intensifies post-ischemic brain inflammation and neuronal death

Double immunohistochemical staining for HMGB1/NeuN and HMGB1/MPO

The qualitative analysis of double immunofluorescent labeling for HMGB1 with NeuN (neuron-specific nuclear protein) or MPO (myeloperoxidase) on the cortical tissue 24 h after MCAO or sham operation showed that (1) the number of neurons immunoreactive to NeuN in the ischemic penumbra decreased more in ADAMTS13KO mice compared to WT (Fig. 2), (2) HMGB1 immunoreactivity disappeared in the ischemic neuronal nuclei in both KO and WT mice, suggestive of a translocation of HMGB1 from neuronal nucleus either to neuronal cytoplasm or to extracellular space (Fig. 2), and (3) cells with co-expression of MPO (a marker for neutrophils, macrophages and/or microglia) and HMGB1 appeared more prominently in the ischemic penumbra in ADAMTS13KO mice than in WT (Fig. 3).

Table 2 Effect of ADAMTS13 gene deletion on regional cerebral blood flow (rCBF) in mice of 30-min MCAO model

	WT ($n = 6$)		KO ($n = 7$)
Time (min)			
Baseline	100.0 ± 0	ns	100.0 ± 0
0	13.6 ± 4.6	ns	13.2 ± 2.0
10	17.9 ± 3.4	ns	22.4 ± 6.3
20	17.7 ± 5.2	ns	19.3 ± 5.7
30	16.8 ± 4.7	ns	18.6 ± 3.5
Reperfusion	114.3 ± 19.1	ns	88.1 ± 8.1
40	90.5 ± 12.7	$p < 0.05$[a]	48.4 ± 8.4
50	93.8 ± 11.3	$p < 0.01$[a]	35.4 ± 7.7
60	83.2 ± 6.8	$p < 0.01$[a]	28.1 ± 4.7
Time (hour)			
24	72.9 ± 13.9	$p < 0.05$[b]	37.2 ± 5.9

rCBF values are expressed as the mean ± SEM (% of baseline)

[a] Turkey-Kramer's test after two-way repeated measures ANOVA [$F(8,98) = 5.841$, $p < 0.0001$)]

[b] Student's t test

Relative fluorescent intensity of NeuN, MPO and HMGB1

The relative fluorescent intensity (%) in the ischemic cerebral cortex 24 h after MCAO was significantly decreased for NeuN in ADAMTS13KO mice compared to WT [57.5 ± 8.7 in KO vs. 93.2 ± 5.5 in WT ($p < 0.05$, student's t test)], and increased for both MPO and HMGB1 more in ADAMTS13KO mice than in WT [KO vs. WT: 557.7 ± 139.8 vs. 310.4 ± 131.7 for MPO, and 159.7 ± 46.5 vs. 70.2 ± 35.1 for HMGB1 (although not statistically significant)].

Discussion

The (UL)VWF, the substrate of ADAMTS13, recruits platelets and leukocytes onto the injured vascular endothelium, and mediates microvascular plugging and enhances the tissue inflammation [5, 7, 30, 37, 40, 41, 43, 44]. ADAMTS13 inhibits these prothrombotic and proinflammatory functions of (UL)VWF [7, 13, 41]. Our current study implies that ADAMTS13 gene deletion amplifies systemic and brain inflammatory responses against brain ischemia–reperfusion enhancing a potent cytokine HMGB1 neurotoxicity, leads to progressive decline of post-ischemic cerebral blood reflow, and exacerbates ischemic brain injury. ADAMTS13 may play a neuroprotective role against inflammation in ischemic stroke.

ADAMTS13 deficiency may promote inflammation by activating platelets, leukocytes, and vascular endothelium after brain ischemia–reperfusion. Responding to ischemia–

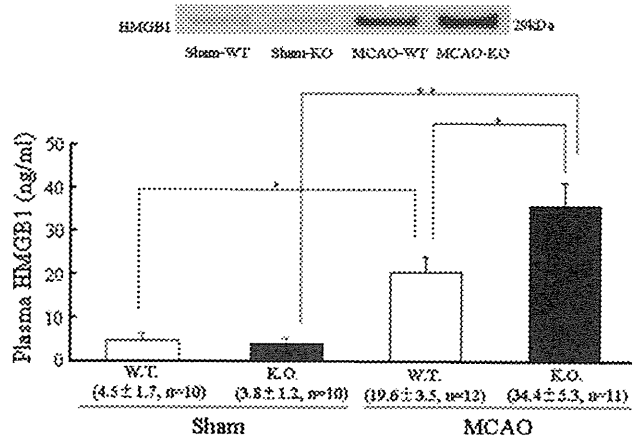

Fig. 1 Effect of ADAMTS13 gene deletion on plasma HMGB1 in mice after 30-min MCAO. The plasma HMGB1 protein was evaluated by western blot. Transient focal ischemia of 30-min MCAO followed by 23.5-h reperfusion significantly increased the plasma HMGB1 level both in ADAMTS13KO and WT mice when compared to sham operation [plasma HMGB1 (ng/ml): MCAO-KO; 34.4 ± 5.3 vs. sham-KO; 3.8 ± 1.2, $p < 0.01$, and MCAO-WT; 19.6 ± 3.5 vs. sham-WT; 4.5 ± 1.7, $p < 0.05$, Tukey–Kramer's test after two-way ANOVA ($F(1,40) = 38.401$, $p < 0.01$)]. This increase of plasma HMGB1 at 24 h after MCAO was more markedly enhanced in ADAMTS13KO mice than in WT [MCAO-KO; 34.4 ± 5.3 vs. MCAO-WT; 19.6 ± 3.5, $p < 0.05$, Tukey–Kramer's test after two-way ANOVA ($F(1,40) = 4.296$, $p < 0.05$)]. Sham-WT $n = 10$, Sham-KO $n = 10$, MCAO-WT $n = 12$, MCAO-KO $n = 11$. Values are expressed as the mean ± SEM. $*p < 0.05$, $**p < 0.01$, Tukey–Kramer's test after two-way ANOVA

reperfusion, the stimulated vascular endothelial cells secrete ULVWF [44]. Binding of VWF to the platelet membrane glycoprotein initiates a signaling cascade that causes platelet activation [25, 46]. The activated platelets release multiple proinflammatory factors, mitogenic mediators, metalloproteinases, and reactive oxygen species, and stimulate the leukocytes and endothelium to incite inflammatory reactions [8, 10]. Further, the platelet–(UL)VWF string directly supports the leukocyte transmigration into the inflammatory tissue [5, 7, 37]. Thus, the VWF-cleaving protease ADAMTS13 plays a role as an anti-inflammatory factor, and therefore its deficiency can exaggerate the post-ischemic inflammation.

In ADAMTS13KO mice after a cerebral ischemia, the plasma HMGB1 increased more and the HMGB1-expressing immune cells appeared more prominent in the cortical penumbra than in WT. The increased extracellular HMGB1 may contribute to secondary ischemic brain damage in ADAMTS13KO mice. The HMGB1, a DNA-binding protein, is a central proinflammatory cytokine [29]. Upon inflammatory signals, the chromosomal HMGB1 relocates into cytoplasmic secretory lysosomes and is secreted into the immunological synapse [29] or into the extracellular space by monocytes/macrophages [45], neutrophils [23], mature dendritic cells [29], natural killer cells

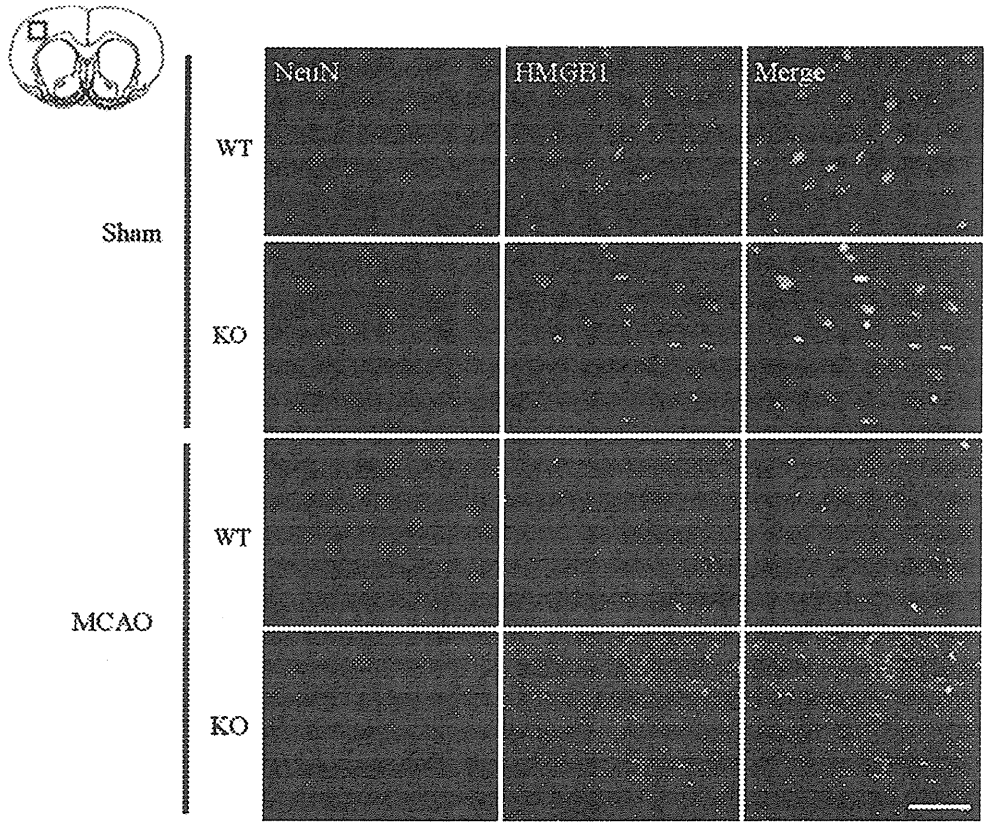

Fig. 2 Effect of ADAMTS13 gene deletion on NeuN positive cells expressing HMGB1 in mice brain after 30-min MCAO. Qualitative analysis of double immunofluorescent labeling for HMGB1 with NeuN on the brain tissue 24 h after MCAO showed that the number of neurons immunoreactive to NeuN in the ischemic cortical penumbra decreased more in ADAMTS13KO mice than WT. The HMGB1 immunoreactivity disappeared in the ischemic neuronal nuclei in both KO and WT mice, suggesting that neuronal-nuclear HMGB1 translocated into either the neuronal cytoplasm or the extracellular space. In addition, the HMGB1 immunoreactivity seemed to increase in the ischemic cortical tissue in the ADAMTS13KO mice, indicating a possibility that non-neuronal HMGB1 positive cells were activated in the KO mice compared to the WT ($n = 5$ in each group). *Scale bar* 50 μm. NeuN positive cells *red*, HMGB1 positive cells *green*, merge *yellow*

[29], and glia [35]. HMGB1 also leaks from necrotic cells [42] and ischemic neurons [38]. The extracellular HMGB1 binds to its receptors, RAGE (receptor for advanced glycation end products) [22], Toll-like receptor 2 (TLR2), and TLR4 [34], recapitulates the intracellular signaling cascades initiated by early proinflammatory stresses, and thus propagates continuous proinflammatory responses [3, 22, 29, 34, 42]. Naturally, high blood HMGB1 correlates with the severity of systemic inflammation [29, 45].

After brain ischemia, extracellular HMGB1 increases rapidly in the blood and central nervous system, and induces neuroinflammation [24, 38]. HMGB-1 early released from the striatal ischemic core can bind to RAGE that is robustly expressed in the peri-infarct region, and extend the ischemic brain injury [38]. HMGB1-RAGE signaling in infiltrating macrophages and activated microglia seemingly mediate neuronal death evolution in the ischemic penumbra [33]. The HMGB1 inhibition in the brain or systemic circulation protects the blood–brain barrier and the brain from ischemia [24, 27, 33, 47]. Inhibition of leukocytes and microglia results in decreased HMGB1 levels in the brain and plasma, reduces apoptosis in the ischemic brain, and improves brain atrophy and neurologic deficits [19, 21]. Therefore, the increased extracellular HMGB1 in the blood and brain of ADAMTS13KO mice as observed in our study can exacerbate ischemic brain injury by intensifying systemic and brain inflammation. Interestingly, the platelet intracellular HMGB1 is exported to the external surface of the plasma membrane upon its activation [39]. Accordingly, the activated platelet may be an additional source of the exceedingly increased plasma HMGB1 in ADAMTS13KO mice after brain ischemia, where enhanced VWF–platelet interactions develop [14]. We suggest that ADAMTS13 deficiency multiplies secondary insults after brain ischemia by up-regulating (UL)VWF-mediating inflammation and enhancing HMGB1 neurotoxicity in the systemic and local environments.

This study suggests a potential therapy with ADAMTS13 for acute ischemic stroke by breaking a vicious circle

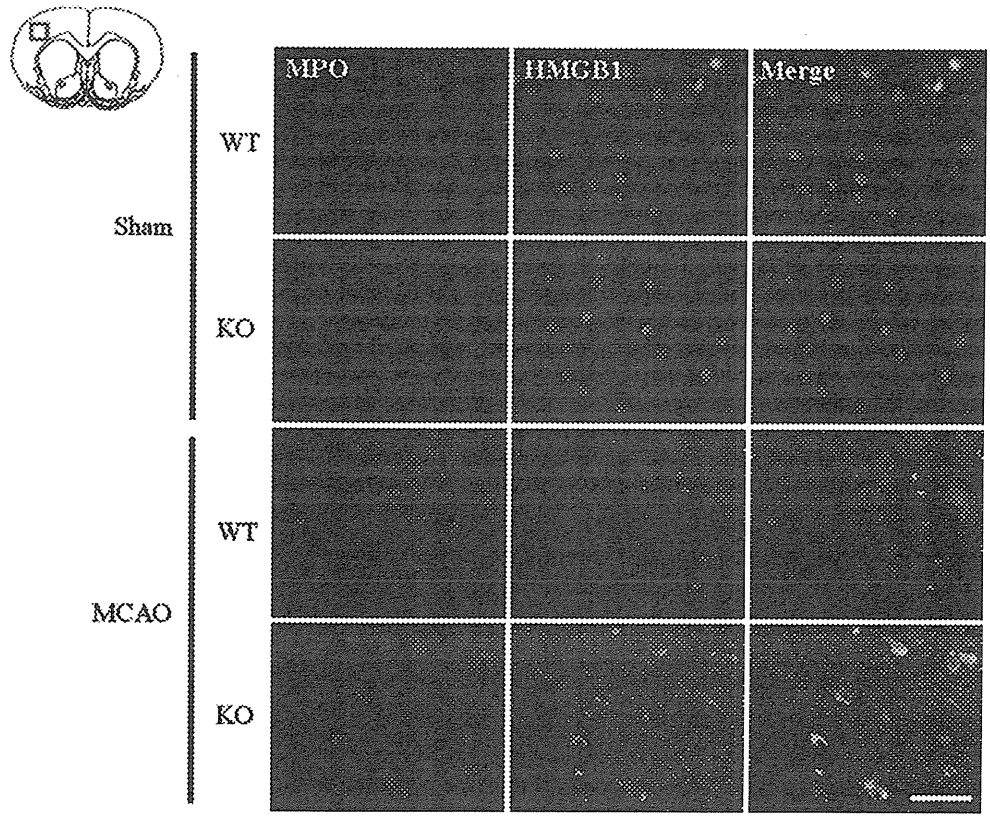

Fig. 3 Effect of ADAMTS13 gene deletion on MPO positive cells expressing HMGB1 in mice brain after 30-min MCAO. Qualitative analysis of double immunofluorescent labeling for HMGB1 with MPO on the brain tissue 24 h after MCAO showed that cells co-expressing MPO and HMGB1 were more prominent in the ischemic cortical penumbra in KO mice than in WT ($n = 5$ in each group). *Scale bar* 50 μm. MPO positive cells *red*, HMGB1 positive cells *green*, merge *yellow*

of thrombosis and inflammation. The (UL)VWF–platelet string interacts with leukocytes, and provokes inflammation [5, 7, 37]. The inflammation induces the endothelial-ULVWF secretion [44]. The proinflammatory cytokines from leukocytes and endothelial cells [such as tumor necrosis factor (TNF)-α and interleukin (IL)-8] stimulate the endothelial ULVWF release and IL-6 protects the ULVWF from cleavage [6]. This would increase the number of ULVWF multimers in plasma sufficiently to aggregate platelets and on vascular endothelial surface to tether platelets and leukocytes onto the endothelium, providing a linkage between thrombosis and inflammation. Of note, HMGB1 stimulates the monocytes/macrophages [3, 34], neutrophils [1, 34] and glial cells [24, 36, 38] to produce TNF-α, IL-1, IL-6 and/or IL-8, and incites the microvascular endothelial cells [12, 38] to express TNF-α, IL-8 and various adhesion molecules. Namely, the increased plasma HMGB1 in ADAMTS13-deficient mice can upregulate ULVWF, and thus reinforce the association between inflammation and thrombosis. ADAMTS13 may prevent stroke evolution by interfering with the crosstalk between thrombosis and inflammation.

Thrombolytic therapy using tissue plasminogen activator (tPA) for acute stroke has limitations in the therapeutic time window and in the drug dosage due to the risk of hemorrhagic transformation [18]. Further, tPA directly exerts neurotoxicity in the ischemic brain [26]. We suggest that a regulation of the interaction between (UL)VWF–platelet and leukocyte using ADAMTS13 may become a novel therapeutic option in acute brain ischemia. ADAMTS13 does not dissolve the VWF–platelet–primary hemostatic thrombus in the absence of pathologically high fluid shear stress. Therefore, ADAMTS13 may be particularly well suited for acute ischemic stroke without increasing hemorrhagic complications. An early experimental study [48] together with our preliminary data (not shown) demonstrated that recombinant human ADAMTS13 administration reduced infarct volume in stroke model in a VWF-dependent manner without producing cerebral hemorrhage.

This study has several limitations. For example, the reduction of cerebral blood reflow in ADAMTS13KO mice after ischemic insult was continuous and higher than that observed in WT. Therefore, even without the amplified inflammation with HMGB1 neurotoxic effects, only the difference in the blood flow recovery might explain the following more deleterious events in the ischemic brain of ADAMTS13-deficient mice compared to WT. The enhanced elevation of the plasma HMGB1 under ADAMTS13 deficiency after brain ischemia might be also explained simply by the more exacerbated brain damage, regardless of the theoretically intensified interactions between the platelet–(UL)VWF strands and the leukocytes without VWF cleaving protease. The future study required to clarify these issues would include chronological data

evaluations in the stroke experiments with permanent ischemic procedure (deleting the reperfusion effect) or with enhancing/inhibiting HMGB1 activities by drugs or genetic manipulations.

Conclusions

A gene deletion of ADAMTS13 renders mice more vulnerable to brain ischemia–reperfusion injury than their wild-type counterparts, when subjected to 30-min MCAO. This preliminary study suggests that ADAMTS13 deficiency may exacerbate systemic and neuronal inflammation after brain ischemia via VWF-dependent pathway, although this remains still hypothetical. Further studies are warranted to better characterize the role of ADAMTS13 in brain ischemia–reperfusion and to provide a novel therapeutic approach for ischemic stroke by regulating VWF-dependent inflammation as well as microvascular plugging.

References

1. Abraham E, Arcaroli J, Carmody A, Wang H, Tracey KJ (2000) HMG-1 as a mediator of acute lung inflammation. J Immunol 165:2950–2954
2. Abumiya T, Fitridge R, Mazur C, Copeland BR, Koziol JA, Tschopp JF, Pierschbacher MD, del Zoppo GJ (2000) Integrin alpha(IIb)beta(3) inhibitor preserves microvascular patency in experimental acute focal cerebral ischemia. Stroke 31:1402–1409
3. Andersson U, Wang H, Palmblad K, Aveberger AC, Bloom O, Erlandsson-Harris H, Janson A, Kokkola R, Zhang M, Yang H, Tracey KJ (2000) High mobility group 1 protein (HMG-1) stimulates proinflammatory cytokine synthesis in human monocytes. J Exp Med 192:565–570
4. Banno F, Kokame K, Okuda T, Honda S, Miyata S, Kato H, Tomiyama Y, Miyata T (2006) Complete deficiency in ADAMTS13 is prothrombotic, but it alone is not sufficient to cause thrombotic thrombocytopenic purpura. Blood 107:3161–3166
5. Bernardo A, Ball C, Nolasco L, Choi H, Moake JL, Dong JF (2005) Platelets adhered to endothelial cell-bound ultra-large von Willebrand factor strings support leukocyte tethering and rolling under high shear stress. J Thromb Haemost 3:562–570
6. Bernardo A, Ball C, Nolasco L, Moake JF, Dong JF (2004) Effects of inflammatory cytokines on the release and cleavage of the endothelial cell-derived ultralarge von Willebrand factor multimers under flow. Blood 104:100–106
7. Chauhan AK, Kisucka J, Brill A, Walsh MT, Scheiflinger F, Wagner DD (2008) ADAMTS13: a new link between thrombosis and inflammation. J Exp Med 205:2065–2074
8. Davi G, Patrono C (2007) Platelet activation and atherothrombosis. N Engl J Med 357:2482–2494
9. Del Zoppo GJ, Schmid-Schonbein GW, Mori E, Copeland BR, Chang CM (1991) Polymorphonuclear leukocytes occlude capillaries following middle cerebral artery occlusion and reperfusion in baboons. Stroke 22:1276–1283
10. Dole VS, Bergmeier W, Mitchell HA, Eichenberger SC, Wagner DD (2005) Activated platelets induce Weibel-Palade-body secretion and leukocyte rolling in vivo: role of P-selectin. Blood 106: 2334–2339
11. Dong JF, Moake JL, Nolasco L, Bernardo A, Arceneaux W, Shrimpton CN, Schade AJ, McIntire LV, Fujikawa K, López JA (2002) ADAMTS-13 rapidly cleaves newly secreted ultralarge von Willebrand factor multimers on the endothelial surface under flowing conditions. Blood 100:4033–4039
12. Fiuza C, Bustin M, Talwar S, Tropea M, Gerstenberger E, Shelhamer JH, Suffredini AF (2003) Inflammation-promoting activity of HMGB1 on human microvascular endothelial cells. Blood 101:2652–2660
13. Fujikawa K, Suzuki H, McMullen B, Chung DP (2001) Purification of human von Willebrand factor-cleaving protease and its identification as a new member of the metalloproteinase family. Blood 98:1662–1666
14. Fujioka M, Hayakawa K, Mishima K, Kunizawa A, Irie K, Higuchi S, Nakano T, Muroi C, Fukushima H, Sugimoto M, Banno F, Kokame K, Miyata T, Fujiwara M, Okuchi K, Nishio K (2010) ADAMTS13 gene deletion aggravates ischemic brain damage: a possible neuroprotective role of ADAMTS13 by ameliorating postischemic hypoperfusion. Blood 115:1650–1653
15. Fujioka M, Taoka T, Matsuo Y, Hiramatsu KI, Sakaki T (1999) Novel brain ischemic change on MRI. Delayed ischemic hyperintensity on T1-weighted images and selective neuronal death in the caudoputamen of rats after brief focal ischemia. Stroke 30:1043–1046
16. Fujioka M, Taoka T, Matsuo Y, Mishima K, Ogoshi K, Kondo Y, Tsuda M, Fujiwara M, Asano T, Sakaki T, Miyasaki A, Park D, Siesjö BK (2003) Magnetic resonance imaging shows delayed ischemic striatal neurodegeneration. Ann Neurol 54:732–747
17. Furlan M, Robles R, Galbusera M, Remuzzi G, Kyrle PA, Brenner B, Krause M, Scharrer I, Aumann V, Mittler U, Solenthaler M, Lammle B (1998) von Willebrand factor-cleaving protease in thrombotic thrombocytopenic purpura and the hemolytic-uremic syndrome. N Engl J Med 339:1578–1584
18. Hacke W, Kaste M, Bluhmki E, Brozman M, Davalos A, Guidetti D, Larrue V, Lees KR, Medeghri Z, Machnig T, Schneider D, von Kummer R, Wahlgren N, Toni D (2008) Thrombolysis with alteplase 3 to 4.5 hours after acute ischemic stroke. N Engl J Med 359: 1317–1329
19. Hayakawa K, Mishima K, Irie K, Hazekawa M, Mishima S, Fujioka M, Orito K, Egashira N, Katsurabayashi S, Takasaki K, Iwasaki K, Fujiwara M (2008) Cannabidiol prevents a post-ischemic injury progressively induced by cerebral ischemia via a high-mobility group box1-inhibiting mechanism. Neuropharmacology 55:1280–1286
20. Hayakawa K, Mishima K, Nozako M, Hazekawa M, Irie K, Fujioka M, Orito K, Abe K, Hasebe N, Egashira N, Iwasaki K, Fujiwara M (2007) Delayed treatment with cannabidiol has a cerebroprotective action via a cannabinoid receptor-independent myeloperoxidase-inhibiting mechanism. J Neurochem 102:1488–1496
21. Hayakawa K, Mishima K, Nozako M, Hazekawa M, Mishima S, Fujioka M, Orito K, Egashira N, Iwasaki K, Fujiwara M (2008) Delayed treatment with minocycline ameliorates neurologic impairment through activated microglia expressing a high-mobility group box1-inhibiting mechanism. Stroke 39:951–958
22. Hori O, Brett J, Slattery T, Cao R, Zhang J, Chen JX, Nagashima M, Lundh ER, Vijay S, Nitecki D et al (1995) The receptor for advanced glycation end products (RAGE) is a cellular binding site for amphoterin. Mediation of neurite outgrowth and co-expression of rage and amphoterin in the developing nervous system. J Biol Chem 270:25752–25761
23. Ito I, Fukazawa J, Yoshida M (2007) Post-translational methylation of high mobility group box 1 (HMGB1) causes its cytoplasmic localization in neutrophils. J Biol Chem 282: 16336–16344

24. Kim JB, Sig Choi J, Yu YM, Nam K, Piao CS, Kim SW, Lee MH, Han PL, Park JS, Lee JK (2006) HMGB1, a novel cytokine-like mediator linking acute neuronal death and delayed neuroinflammation in the postischemic brain. J Neurosci 26:6413–6421
25. Kroll MH, Harris TS, Moake JL, Handin RI, Schafer AI (1991) von Willebrand factor binding to platelet GpIb initiates signals for platelet activation. J Clin Invest 88:1568–1573
26. Liu D, Cheng T, Guo H, Fernandez JA, Griffin JH, Song X, Zlokovic BV (2004) Tissue plasminogen activator neurovascular toxicity is controlled by activated protein C. Nat Med 10: 1379–1383
27. Liu K, Mori S, Takahashi HK, Tomono Y, Wake H, Kanke T, Sato Y, Hiraga N, Adachi N, Yoshino T, Nishibori M (2007) Anti-high mobility group box 1 monoclonal antibody ameliorates brain infarction induced by transient ischemia in rats. FASEB J 21:3904–3916
28. Lo EH, Dalkara T, Moskowitz MA (2003) Mechanisms, challenges and opportunities in stroke. Nat Rev Neurosci 4:399–415
29. Lotze MT, Tracey KJ (2005) High-mobility group box 1 protein (HMGB1): nuclear weapon in the immune arsenal. Nat Rev Immunol 5:331–342
30. Moake JL, Rudy CK, Troll JH, Weinstein MJ, Colannino NM, Azocar J, Seder RH, Hong SL, Deykin D (1982) Unusually large plasma factor VIII: von Willebrand factor multimers in chronic relapsing thrombotic thrombocytopenic purpura. N Engl J Med 307:1432–1435
31. Mori E, del Zoppo GJ, Chambers JD, Copeland BR, Arfors KE (1992) Inhibition of polymorphonuclear leukocyte adherence suppresses no-reflow after focal cerebral ischemia in baboons. Stroke 23:712–718
32. Mori T, Town T, Tan J, Tateishi N, Asano T (2005) Modulation of astrocytic activation by arundic acid (ONO-2506) mitigates detrimental effects of the apolipoprotein E4 isoform after permanent focal ischemia in apolipoprotein E knock-in mice. J Cereb Blood Flow Metab 25:748–762
33. Muhammad S, Barakat W, Stoyanov S, Murikinati S, Yang H, Tracey KJ, Bendszus M, Rossetti G, Nawroth PP, Bierhaus A, Schwaninger M (2008) The HMGB1 receptor RAGE mediates ischemic brain damage. J Neurosci 28:12023–12031
34. Park JS, Svetkauskaite D, He Q, Kim JY, Strassheim D, Ishizaka A, Abraham E (2004) Involvement of toll-like receptors 2 and 4 in cellular activation by high mobility group box 1 protein. J Biol Chem 279:7370–7377
35. Passalacqua M, Patrone M, Picotti GB, Del Rio M, Sparatore B, Melloni E, Pontremoli S (1998) Stimulated astrocytes release high-mobility group 1 protein, an inducer of LAN-5 neuroblastoma cell differentiation. Neuroscience 82:1021–1028
36. Pedrazzi M, Patrone M, Passalacqua M, Ranzato E, Colamassaro D, Sparatore B, Pontremoli S, Melloni E (2007) Selective proinflammatory activation of astrocytes by high-mobility group box 1 protein signaling. J Immunol 179:8525–8532
37. Pendu R, Terraube V, Christophe OD, Gahmberg CG, de Groot PG, Lenting PJ, Denis CV (2006) P-selectin glycoprotein ligand 1 and beta2-integrins cooperate in the adhesion of leukocytes to von Willebrand factor. Blood 108:3746–3752
38. Qiu J, Nishimura M, Wang Y, Sims JR, Qiu S, Savitz SI, Salomone S, Moskowitz MA (2008) Early release of HMGB-1 from neurons after the onset of brain ischemia. J Cereb Blood Flow Metab 28:927–938
39. Rouhiainen A, Imai S, Rauvala H, Parkkinen J (2000) Occurrence of amphoterin (HMG1) as an endogenous protein of human platelets that is exported to the cell surface upon platelet activation. Thromb Haemost 84:1087–1094
40. Ruggeri ZM (2007) The role of von Willebrand factor in thrombus formation. Thromb Res 120(Suppl 1):S5–S9
41. Sadler JE (2008) Von Willebrand factor, ADAMTS13, and thrombotic thrombocytopenic purpura. Blood 112:11–18
42. Scaffidi P, Misteli T, Bianchi ME (2002) Release of chromatin protein HMGB1 by necrotic cells triggers inflammation. Nature 418:191–195
43. Siedlecki CA, Lestini BJ, Kottke-Marchant KK, Eppell SJ, Wilson DL, Marchant RE (1996) Shear-dependent changes in the three-dimensional structure of human von Willebrand factor. Blood 88:2939–2950
44. Vischer UM (2006) von Willebrand factor, endothelial dysfunction, and cardiovascular disease. J Thromb Haemost 4:1186–1193
45. Wang H, Bloom O, Zhang M, Vishnubhakat JM, Ombrellino M, Che J, Frazier A, Yang H, Ivanova S, Borovikova L, Manogue KR, Faist E, Abraham E, Andersson J, Andersson U, Molina PE, Abumrad NN, Sama A, Tracey KJ (1999) HMG-1 as a late mediator of endotoxin lethality in mice. Science 285:248–251
46. Yin H, Liu J, Li Z, Berndt MC, Lowell CA, Du X (2008) Src family tyrosine kinase Lyn mediates VWF/GPIb-IX-induced platelet activation via the cGMP signaling pathway. Blood 112: 1139–1146
47. Zhang J, Takahashi HK, Liu K, Wake H, Liu R, Maruo T, Date I, Yoshino T, Ohtsuka A, Mori S, Nishibori M (2011) Anti-high mobility group box-1 monoclonal antibody protects the blood–brain barrier from ischemia-induced disruption in rats. Stroke 42:1420–1428
48. Zhao BQ, Chauhan AK, Canault M, Patten IS, Yang JJ, Dockal M, Scheiflinger F, Wagner DD (2009) von Willebrand factor-cleaving protease ADAMTS13 reduces ischemic brain injury in experimental stroke. Blood 114:3329–3334

ultrastructural and functional characterization. *J Thromb Haemost* 2010; **8**: 173–84.
13 Mangin P, Yap CL, Nonne C, Sturgeon SA, Goncalves I, Yuan Y, Schoenwaelder SM, Wright CE, Lanza F, Jackson SP. Thrombin overcomes the thrombosis defect associated with platelet GPVI/FcRgamma deficiency. *Blood* 2006; **107**: 4346–53.
14 Kalia N, Auger JM, Atkinson B, Watson SP. Critical role of FcR gamma-chain, LAT, PLCgamma2 and thrombin in arteriolar thrombus formation upon mild, laser-induced endothelial injury *in vivo*. *Microcirculation* 2008; **15**: 325–35.
15 Konstantinides S, Ware J, Marchese P, Mus-Jacobs F, Loskutoff DJ, Ruggeri ZM. Distinct antithrombotic consequences of platelet glycoprotein Ibalpha and VI deficiency in a mouse model of arterial thrombosis. *J Thromb Haemost* 2006; **4**: 2014–21.
16 Massberg S, Gawaz M, Gruner S, Schulte V, Konrad I, Zohlnhofer D, Heinzmann U, Nieswandt B. A crucial role of glycoprotein VI for platelet recruitment to the injured arterial wall *in vivo*. *J Exp Med* 2003; **197**: 41–9.
17 Eckly A, Hechler B, Freund M, Zerr M, Cazenave JP, Lanza F, Mangin PH, Gachet C. Mechanisms underlying FeCl(3) -induced arterial thrombosis. *J Thromb Haemost* 2011; **9**: 779–89.
18 Inoue O, Suzuki-Inoue K, McCarty OJ, Moroi M, Ruggeri ZM, Kunicki TJ, Ozaki Y, Watson SP. Laminin stimulates spreading of platelets through integrin alpha6beta1-dependent activation of GPVI. *Blood* 2006; **107**: 1405–12.
19 Brill A. A ride with ferric chloride. *J Thromb Haemost* 2011; **9**: 776–8.
20 Wong LC, Langille BL. Developmental remodeling of the internal elastic lamina of rabbit arteries: effect of blood flow. *Circ Res* 1996; **78**: 799–805.
21 Marsh LE, Lewis SD, Lehman ED, Gardell SJ, Motzel SL, Lynch JJ Jr. Assessment of thrombin inhibitor efficacy in a novel rabbit model of simultaneous arterial and venous thrombosis. *Thromb Haemost* 1998; **79**: 656–62.
22 Pinel C, Wice SM, Hiebert LM. Orally administered heparins prevent arterial thrombosis in a rat model. *Thromb Haemost* 2004; **91**: 919–26.
23 Wang X, Cheng Q, Xu L, Feuerstein GZ, Hsu MY, Smith PL, Seiffert DA, Schumacher WA, Ogletree ML, Gailani D. Effects of factor IX or factor XI deficiency on ferric chloride-induced carotid artery occlusion in mice. *J Thromb Haemost* 2005; **3**: 695–702.
24 Pozgajova M, Sachs UJ, Hein L, Nieswandt B. Reduced thrombus stability in mice lacking the alpha2A-adrenergic receptor. *Blood* 2006; **108**: 510–4.

von Willebrand factor-to-ADAMTS13 ratio increases with age in a Japanese population

K. KOKAME,* T. SAKATA,† Y. KOKUBO‡ and T. MIYATA*
**Department of Molecular Pathogenesis, †Laboratory of Clinical Chemistry* and *‡Department of Preventive Cardiology, National Cerebral and Cardiovascular Center, Suita, Osaka, Japan*

To cite this article: Kokame K, Sakata T, Kokubo Y, Miyata T. von Willebrand factor-to-ADAMTS13 ratio increases with age in a Japanese population. *J Thromb Haemost* 2011; **9**: 1426–8.

ADAMTS13, a plasma metalloprotease, regulates platelet aggregation through shear stress-dependent specific cleavage of von Willebrand factor (VWF) multimers. Severe deficiency of plasma ADAMTS13 activity results in accumulation of unusually high-molecular-weight VWF multimers in plasma, and can cause a systemic disease, thrombotic thrombocytopenic purpura (TTP) [1–3]. Previously, we developed a simple and quantitative assay for measuring ADAMTS13 activity using FRETS-VWF73, a fluorogenic peptide substrate [4]. In this study, we used the assay to measure plasma ADAMTS13 activity in 3616 individuals from the Japanese general population.

We used plasma samples from the previously published Suita Study [5–7], an epidemiological study consisting of randomly selected Japanese residents of the city of Suita, which is located in the second largest urban area in Japan. Participants between the ages of 30 and 79 years were randomly selected from the municipality population registry and stratified into groups by sex and age in 10-year increments in 1989. They underwent regular health check-ups between September 1989 and March 1994. Subjects have continued to visit the National Cerebral and Cardiovascular Center every 2 years for regular health check-ups. Our study protocol was approved by the ethical review committee, and only subjects who provided written informed consent for genetic analyses were included.

When the mean of all plasma ADAMTS13 activity values was set at 100%, the standard deviation (SD) was 27% (Fig. 1A). The fifth percentile, 25th percentile, median, 75th percentile and 95th percentile were 61%, 81%, 97%, 116% and 148%, respectively. The mean activity of men (93 ± 24%, mean ± SD, n = 1687) was significantly lower (P < 0.0001) than that of women (106 ± 27%, n = 1929), consistent with the previous report [4].

In both men and women, the plasma ADAMTS13 activity tended to decrease with age, especially after age 60 (Fig. 1B). A linear regression model also indicated the decrease with age (regression coefficient of −0.642 and 95% confidence intervals (CI) of −0.740 to −0.544 in men; −0.663 and −0.767 to −0.558 in women). We also measured plasma VWF antigen levels

Correspondence: Koichi Kokame, Department of Molecular Pathogenesis, National Cerebral and Cardiovascular Center, 5-7-1 Fujishirodai, Suita, Osaka 565-8565, Japan.
Tel.: +81 6 6833 5012; fax: +81 6 6835 1176.
E-mail: kame@ri.ncvc.go.jp

DOI: 10.1111/j.1538-7836.2011.04333.x

Received 30 March 2011, accepted 24 April 2011

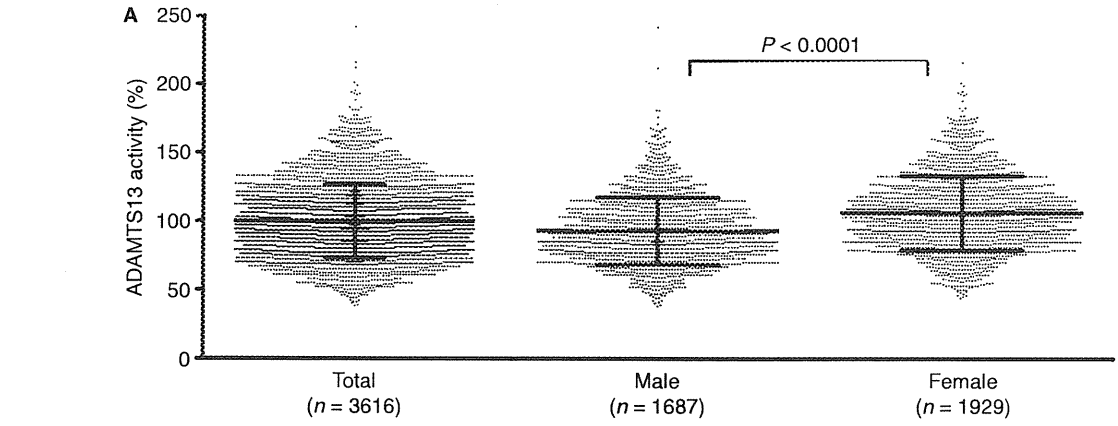

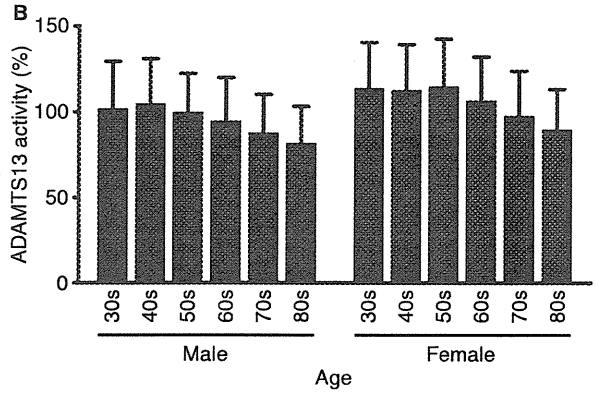

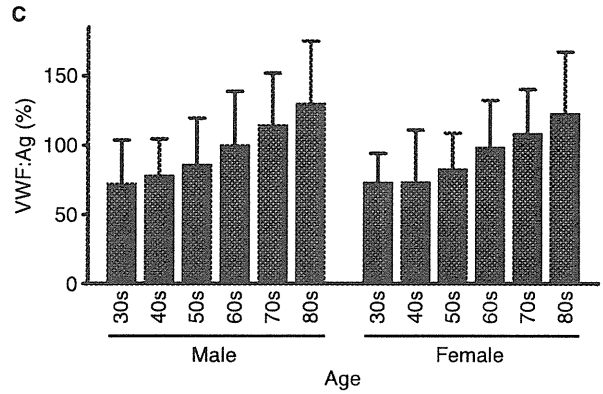

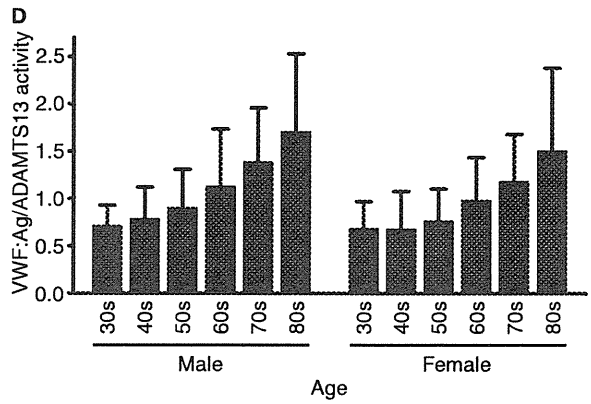

E

		Q1	Q2	Q3	Q4
Male $n = 1687$	ADAMTS13 activity (%)	38–76	76–90	90–109	109–242
	VWF:Ag (%) ± SE	107 ± 11	106 ± 11	108 ± 11	111 ± 11
		$P = 0.153$			
Female $n = 1929$	ADAMTS13 activity (%)	44–86	86–104	104–123	123–216
	VWF:Ag (%) ± SE	103 ± 9	99 ± 10	99 ± 10	101 ± 9
		$P = 0.670$			

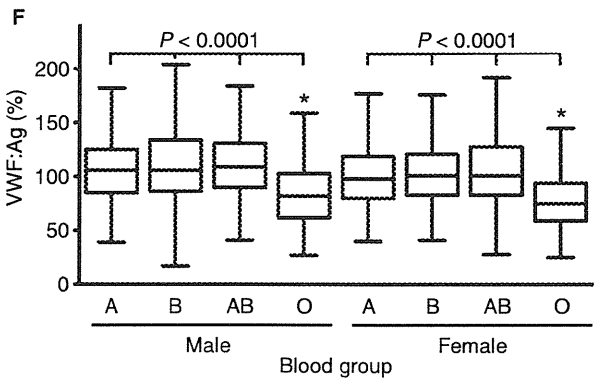

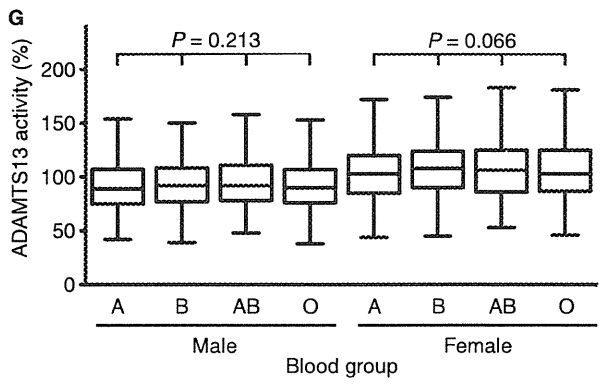

Fig. 1. Plasma ADAMTS13 activity in a Japanese general population. (A) Scatter dot plot of total, male and female plasma ADAMTS13 activity. The mean of all values was set at 100%. Lines indicate the means with SD. *P*, *t*-test. (B, C, D) Age-specific ADAMTS13 activity (B), VWF:Ag (C) and VWF:Ag-to-ADAMTS13 activity ratio (D). The mean of all VWF:Ag values was set at 100%. Error bars indicate SD. (E) Analysis of VWF:Ag by quartiles of plasma ADAMTS13 activity. *P*, ANCOVA. (F, G) Box-and-whisker plot of blood group-specific VWF:Ag (F) and ADAMTS13 activity (G). *P*, Kruskal–Wallis test. *Only blood group O had significantly different VWF:Ag from other blood groups.